October 21, 2013

FINAL REPORT

Modelling Study of Iron and Manganese in Groundwater

Submitted to:
Catherine Schachtel
Society of Contaminated Sites Approved Professionals of BC
613-744 Hastings Street, Vancouver, BC
V6C 1A5

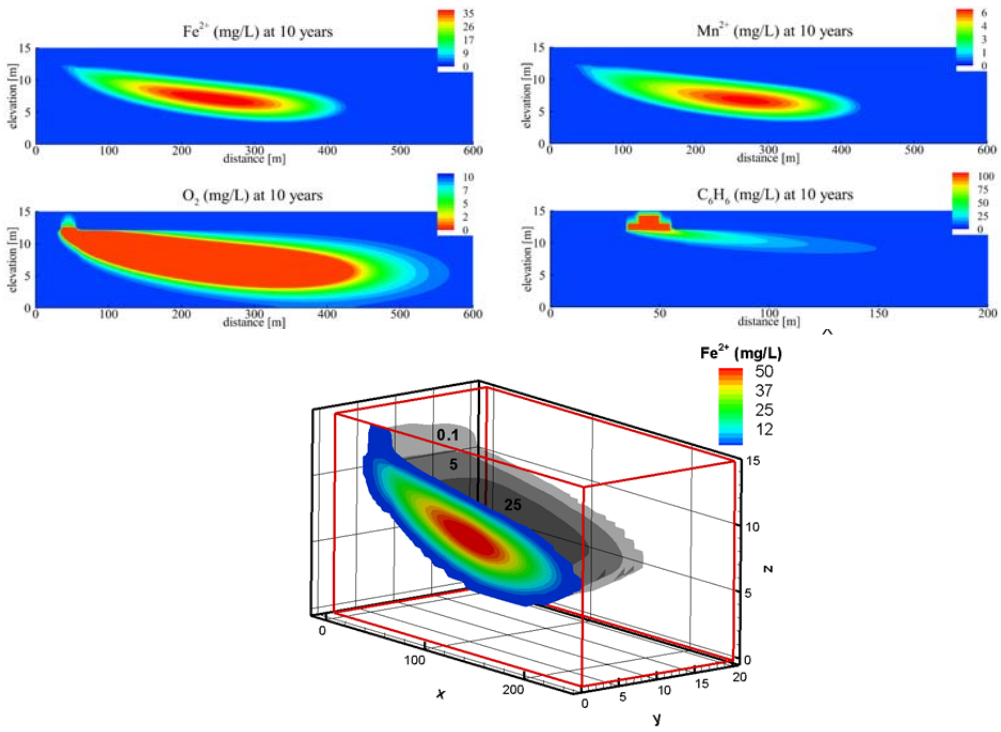

Report **Number:** 1214360089-001-R-Rev0

Distribution:

2 copies - CSAP

2 copies - Golder Associates

REPORT

Golder Associates

SUMMARY

This report, prepared by Golder Associates Ltd. (Golder) for the Society of Contaminated Sites Approved Professionals (CSAP) of British Columbia, is an applied research study on iron and manganese in groundwater system. Iron and manganese are of importance in British Columbia because concentrations of these substances in groundwater may be elevated above background levels because of biological and geochemical processes associated with organic chemicals and therefore may be of potential concern to human health and/or the environment. The purpose of this study is to evaluate the fate and transport of iron and manganese in groundwater through primarily a numerical modeling study conducted using the MIN3P-Dusty code (Mayer *et al.*, 2002 and Molins and Mayer, 2007).

Anaerobic or anoxic groundwater conditions exist at many sites with either anthropogenic or naturally-occurring organic substances. Examples of anthropogenic chemicals that result in depleted oxygen in groundwater systems include petroleum hydrocarbons, landfill leachate, and creosote or coal tar. Anoxic conditions and biodegradation of organics within source zones result in the reductive dissolution of iron and manganese in soil minerals causing iron and manganese groundwater plumes. As the iron and manganese plume moves down-gradient, there is a transition to an aerobic geochemical regime where the iron and manganese tends to oxidize and precipitate.

A modeling study of reactive transport of petroleum hydrocarbons (benzene) and redox species including iron and manganese was completed. The results highlight the importance of the combination of contamination source characteristics, geochemical factors and hydrogeologic conditions on iron and manganese fate and transport. The importance of primary and secondary oxidation-reduction reactions on dissolved iron and manganese plumes and role of oxygen and redox conditions as indicators of their persistence is demonstrated.

A comparison of the plume lengths at 10 years simulation time shows that the dissolved iron and manganese plumes extend further from the source than the benzene plume with plume length ratios ranging from 1.4 to 3.8 for the scenarios considered. Once the petroleum hydrocarbon source zone is depleted, the dissolved benzene is rapidly attenuated (within six months), but the elevated iron and manganese in groundwater persists at similar concentrations to pre-depletion conditions for over five years. The predicted iron and manganese concentrations within anoxic plumes exceed drinking water standards in the BC Contaminated Sites Regulation.

The modeling results suggest that iron and manganese plumes may be more extensive than petroleum hydrocarbon plumes and that elevated concentrations may persist for an extended period of time after hydrocarbon sources are removed. However, the predicted iron and manganese plume lengths are likely conservative because certain processes (that are challenging to model because of limited data) such as sorption of reduced iron or precipitation of iron sulphides were not included. A literature search indicated that there are site conditions, depending on the case study, where the plume lengths are similar to the modeling results (longer iron and manganese than benzene, toluene, ethylbenzene and xylenes (BTEX) plumes), as well as conditions where plume lengths of iron and BTEX compounds are well correlated.

An inference from the modeling results and case studies is that larger petroleum hydrocarbon source zones and conditions where groundwater is anoxic because of anthropogenic (*e.g.*, landfill) or natural conditions will have greater potential for longer dissolved iron and manganese plumes. For smaller sources representative of many petroleum hydrocarbon releases at gasoline station sites there is expected to be less potential for significant impacts to drinking water from iron and manganese based on modeling results for scenarios where a smaller hydrocarbon source or source removal were simulated, which predicted lower iron and manganese concentrations.

ACKNOWLEDGMENTS

The direction of Ms. Catherine Schachtel, executive director of the CSAP Society and excellent review comments by the CSAP Task Group, Dr. Greg Sutherland, Dr. Reidar Zapf-Gilje and Mr. Guy Patrick, are gratefully acknowledged. The assistance and advice of the author of the MIN3P model, Dr. Ulrich Mayer of the University of British Columbia, is gratefully acknowledged.

DISCLAIMER

This report provides a modeling study of iron and manganese fate and transport in groundwater and has been prepared by Golder Associates Ltd. for the CSAP Society of British Columbia. Any use that a third party may make of this report, or any reliance on or decisions made based on it, are the responsibility of the third parties. We disclaim responsibility or consequential financial effects on site management, or requirements for follow-up actions and costs.

The services performed as described in this report were conducted in a manner consistent with the level of care and skill normally exercised by other members of the science professions currently practicing under similar conditions, subject to the time limits and financial and physical constraints applicable to the services. This report provides professional opinions and, therefore, no warranty is expressed, implied, or made as to the conclusions, advice, and recommendations offered in this report. This report does not provide a legal opinion regarding compliance with applicable laws or regulations, and should not be construed to represent regulatory policy.

TABLE OF CONTENTS

TABLES

FIGURES

APPENDICES

APPENDIX A

Scenario 1 Gas Phase Concentrations And Reaction Rates

1.0 OBJECTIVES

Golder Associates Ltd. (Golder) was retained by the Society of Contaminated Sites Approved Professionals of British Columbia to conduct an applied research study on iron and manganese issues in groundwater. Iron and manganese are of importance in British Columbia because concentrations of these substances in groundwater may be elevated above background levels because of biological and geochemical processes associated with organic chemicals and therefore may be of potential concern to human health and/or the environment.

Anaerobic or anoxic groundwater conditions exist at many sites with either anthropogenic or naturally-occurring organic substances. Examples of anthropogenic chemicals that result in depleted oxygen in groundwater systems include petroleum hydrocarbons, landfill leachate, and creosote or coal tar. Anoxic conditions and biodegradation of organics within source zones result in the reductive dissolution of iron and manganese in soil minerals causing iron and manganese groundwater plumes. As the iron and manganese plume moves down-gradient, there is a transition to an aerobic geochemical regime where the iron and manganese tends to precipitate.

The purpose of this study is to evaluate the fate and transport of iron and manganese in groundwater through primarily a numerical modeling study conducted using the MIN3P-Dusty code (Mayer *et al.*, 2002). A literature review of fate and transport processes and available field data on iron and manganese was also completed. The objectives of the program are as follows:

- Better understand natural attenuation processes of iron and manganese at sites with organic contamination;
- Evaluate the lateral extent of iron and manganese groundwater plumes relative to the extent of petroleum hydrocarbon plumes;
- Evaluate the longevity of iron and manganese plumes once petroleum hydrocarbon source zones are remediated or removed;
- Compare predicted iron and manganese concentrations to drinking water standards in the BC Contaminated Sites Regulation (CSR).

A secondary objective of this study is to identify possible risk management measures for iron and manganese when concentrations are of potential concern.

The modeling scope is comprehensive and six scenarios describing different contamination sources and processes were simulated using the MIN3P-Dusty model. Both two-dimensional and three-dimensional numerical simulations were completed. Given the complexity in the modeling, an extensive sensitivity analysis of multiple input parameters was beyond the scope of this work.

This study is relevant given the prevalence of iron and manganese in groundwater at contaminated sites in British Columbia and lack of comprehensive studies of the fate and transport of these compounds in the literature.

2.0 REGULATORY BACKGROUND

In British Columbia, there are Generic Numerical Water Standards in the BC Contaminated Sites Regulation (CSR) for four defined uses consisting of protection of groundwater used for drinking water (DW), groundwater discharging to aquatic water bodies (AW), groundwater used for irrigation (IW), and groundwater used for livestock watering (LW).

For iron and manganese there are CSR standards for drinking water, which are 6,500 ug/L for iron and 550 ug/L for manganese, and for irrigation water, which are 5,000 ug/L for iron and 200 ug/L for manganese. The drinking water standards for iron and manganese are toxicologically-based standards derived by the BC Ministry of Environment for human health protection. There are no iron and manganese standards for aquatic life protection, but when groundwater with elevated iron and manganese concentrations discharges to a surface water body, the possible effects of acid generation and oxide precipitation on aquatic life may require evaluation in accordance with the BC Environmental Management Act, federal Fisheries Act, or other applicable legislation.

Stage 8 amendments to the CSR came into effect on January 24, 2013. The amendments modify the Generic Numerical Water Standards for iron and manganese in Schedules 6 and 10 of the Regulation, and restrict the application of the water standards for iron and manganese to sites with specific activities that used iron and manganese, defined as a specific subset of the activities listed in Schedule 2 of the CSR. From the activities listed, the iron and manganese water standards would not apply at petroleum hydrocarbon (fuel) distribution or service station sites.

3.0 CONCEPTUAL SITE MODEL

The conceptual site model for iron and manganese fate and transport is described through an overview of processes, a detailed discussion of oxidation-reduction reactions, review of select modeling and field case studies.

3.1 Overview of Processes

The conceptual model for this study begins with a light non-aqueous phase liquid (LNAPL) source consisting of petroleum hydrocarbons, which for numerical simulations presented in this report is assumed to be gasoline. When LNAPL is released in the vadose zone, the LNAPL moves predominantly downward as a separate immiscible phase under the influence of gravity, until it encounters the water table, where buoyancy forces and capillary forces due to higher water contents result in vertical accumulation and lateral spreading of the LNAPL. Residual LNAPL remains within the vadose zone in the zone of LNAPL migration. At the water table, the repeated rising and falling of the water table often results in the formation of a LNAPL smear zone.

For the above conceptual source model, the fate and transport of organic and inorganic constituents will be controlled by physical, biological, and geochemical processes and reactions involving mineral, petroleum hydrocarbon (immiscible phase), aqueous and gaseous constituents. For conceptualization purposes, the aqueous and gaseous phases are considered mobile, and the solid phase is immobile. The aqueous phase consists of inorganic and organic dissolved species and water itself, while the gaseous phase is composed of gases common to the atmosphere and water vapour, but may also include other gases such as methane, carbon dioxide, hydrogen sulfide and petroleum hydrocarbon compounds in gaseous form. The solid phase is comprised of LNAPL, minerals, amorphous phases, and organic matter (Mayer *et al.*, 2002).

Subsurface fate and transport processes may include:

- dissolution of petroleum hydrocarbon compounds in the LNAPL source; in the vadose zone this occurs because of infiltrating water and in the smear zone (below the water table) because of flowing groundwater;
- dissolution and precipitation of inorganic constituents (minerals);
- advective-dispersive transport of solutes in flowing groundwater;
- volatilization of petroleum hydrocarbon compounds from LNAPL and dissolved hydrocarbon;
- gas-exchange at the water table, for example, exchange between gaseous and dissolved oxygen;
- microbial mediated oxidation-reduction reactions;
- aqueous and surface complexation reactions;
- adsorption or absorption of petroleum hydrocarbon compounds and inorganic constituents onto or into aquifer materials, for example, absorption of hydrocarbons into organic matter and adsorption of inorganic constituents onto organic matter and/or minerals,
- ion exchange, and
- aqueous and gas-phase diffusion.

Reactions involving these constituents may occur within a single phase (homogeneous reactions) or may involve constituents from two or more phases (heterogeneous reactions) (*e.g.*, Rubin, 1983). Homogeneous reactions within the aqueous phase include aqueous oxidation-reduction and complexation reactions. Heterogeneous reactions result in mass transfer between the phases and include hydrocarbon LNAPL dissolution, mineral dissolution-precipitation, oxidation-reduction reactions involving solid and dissolved species, ion exchange and gas exchange. Microbial-mediated oxidation-reduction reactions are typically considered to be controlled by rate kinetics, while dissolution-precipitation reactions may or may not be kinetically rate-limiting depending on transport considerations (*e.g.*, how fast is groundwater flowing and how large is the LNAPL source?). Gas exchange, volatilization, complexation and ion exchange processes are typically described as equilibrium processes.

Microbial or oxidation-reduction (redox) reactions are a key process evaluated in this study and are described by both primary reactions involving the biodegradation of petroleum hydrocarbon compounds under aerobic and anaerobic conditions, and secondary reactions involving oxidation of the products of the primary reactions. The redox reactions are controlled by the availability of the terminal electron acceptors (TEAs) and substrate (petroleum hydrocarbon) availability. For example, the biodegradation reactions can be defined as first-order with respect to the substrate or contain a Monod-type dependence, or inhibition terms, or any combination of these terms. Microbial growth and substrate consumption rates are often described by a Monod kinetic model, as follows:

$$R = -\frac{dC}{dt} = \frac{u_{max} C M_t}{K_c + C}$$

Where C is the substrate concentration (mg/L), M_t is the biomass concentration (mg/L), μ_{max} is the substrate utilization rate (sec^{-1}) and K_c is the half-saturation coefficient (mg/L). Literature values are typically adopted for the [$\mu_{max}M_t$] term.

Figure 1 describes the Monod kinetic model. At lower substrate concentrations, the Monod model converges to a first-order decay model; in contrast at higher substrate concentrations, the model converges to a zero-order (constant) decay model. Using a first-order kinetic model where the substrate concentration is higher than K_c will lead to over prediction of the biodegradation rate.

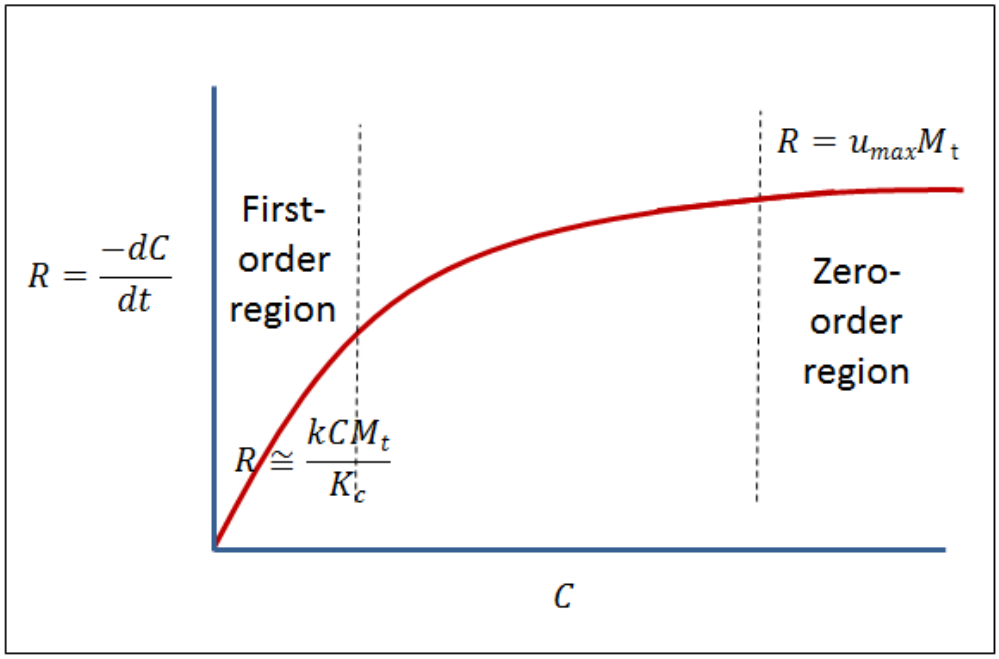

Figure 1: Monod Biodegradation Model.

More complex kinetic models can be adopted including a dual-Monod model, which includes both oxygen and hydrocarbon in the rate definition, and formulations that include biomass growth and decay estimates (Kissel, 1985).

3.2 Oxidation-Reduction Reactions

Microbial metabolism and oxidation of organic carbon is closely tied to the inorganic redox chemistry of groundwater systems (Hunter *et al.*, 1998). Microorganisms derive their energy from oxidative breakdown (loss of electrons) of either anthropogenic carbon (*e.g.*, petroleum hydrocarbon compounds, landfill leachate) or native organic carbon. The principal metabolic pathways are aerobic respiration, denitrification, manganese reduction, iron reduction, sulfate reduction and fermentation (Hunter *et al.*, 1998). The terminal electron acceptors utilized in the five respiratory pathways listed above are oxygen (O_2), nitrate (NO_3^-), manganese oxides (Mn^{3+}, Mn^{4+}), iron oxyhydroxides (Fe^{3+}) and sulphate (SO_4^{2-}) (Wiedemeier *et al.*, 1998; Madigan *et al.*, 2010). During fermentation, the compound being biodegraded serves as both the electron donor (partially reduced) and

electron acceptor (partially oxidized). The intermediate products of fermentation are acetate and hydrogen, which are used as energy substrates by other organisms. The final products of fermentation are carbon dioxide and methane (Van Cappellen and Wang, 1996).

The energy gained by microorganisms through oxidation-reduction reactions depends on the electron acceptor (Table 1). Because aerobic respiration is the most energetically favourable reaction, oxygen is the first electron acceptor utilized in the oxidative process. If dissolved oxygen is depleted, other terminal electron acceptors, such as nitrate, manganese (Mn^{4+}), ferric iron (Fe^{3+}) and sulphate may be used by microorganisms depending on their availability and potential energy yield, or methanogenesis (fermentation) of petroleum hydrocarbons can occur under highly reducing conditions. Oxygen is the TEA from which microorganisms derive the greatest energy, while the least energy is derived through methanogenesis (Table 1). The differences in electron acceptor availability and energy yields of these reactions can lead to spatial separation of the zones in which each degradative pathway dominates (Van Cappellen and Wang, 1996). Christensen *et al.* (2000) present redox monitoring data for two landfills with organic leachate where there are a sequence of zones emanating from the leachate source progressing from methanogenic, sulphate-reducing, iron- and manganese-reducing and finally to nitrate-reducing furthest from the landfill for the Vejen landfill, and progressing from methanogenic and sulphate-reducing, iron-reducing, iron/manganese-reducing, manganese-reducing, manganese/nitrate-reducing to nitrate-reducing for the Grindsted landfill.

Table 1: Typical Redox Potentials for TEAs.

Reaction	Typical redox potential (Eh volt)	Electron acceptor	End product
Oxygen reduction	+0.80 to +0.20	O_2	H_2O, CO_2
Nitrate reduction/nitrate respiration	+0.40 to -0.20	NO_3	NO_2, N_2
Iron reduction	+0.05 to -0.60	Fe_2O_3	Fe, O
Sulphate reduction	-0.10 to -0.75	SO_4	HS
Methanogenesis	-0.20 to -0.80	CO_2	CH_4

Note: From Testa & Jacobs (2004)

The oxidation-reduction of iron and manganese will depend on the availability of oxidized iron and manganese in the soil particles as well as the supply rates of dissolved oxidants in flowing groundwater. The mineralogy, crystal structure and surface area have all been shown to affect the reactivities of iron and manganese oxides (Van Cappellen and Wang, 1996; Postma, 1993). Closely tied to the oxidative reactions of organic substrates, are secondary reactions involving the oxidation of reduced inorganic compounds (*e.g.*, hydrogen (H_2), hydrogen sulphide (H_2S), Fe^{2+}, NH_4^+) by chemolithotrophic bacteria (Chapelle, 1993). For example, dissolved iron (Fe^{2+}) may be re-oxidized when mixed with oxygen-rich groundwater in the fringe areas of the dissolved plume (Christensen *et al.*, 2000). Similarly methane may be re-oxidized when in contact with ferric oxides. Within the core of the plume, reduced iron may also be precipitated through reaction with sulphide, if present.

The geochemical conditions affecting oxidation-reduction reactions are also influenced by geologic heterogeneity and soil deposits of differing properties, which adds complexity to the conceptual site model. Permeability contrasts between aquifers and aquitards can result in anaerobic and fermentative conditions in fine-grained units, and where fermentation products (*e.g.*, hydrogen, acetate) slowly diffuse out of the aquitard. Within the aquifer, the faster flowing groundwater may be oxygenated, and different micro-organisms may

consume these products (Van Cappellen and Wang, 1996). On the other hand, oxygen initially contained in a low permeability (fine grained) soil can diffuse into the reducing plume that moves preferentially through the more permeable (coarse grained) soil and result in enhanced attenuation of the hydrocarbon contaminant and the dissolved Fe^{2+} and Mn^{2+}.

3.3 Review of Previous Modeling Studies

3.3.1 Mayer et al. (2002)

Mayer *et al.* (2002) present results of numerical model simulations of multicomponent reactive transport of organic and inorganic chemicals using the MIN3P model. The general kinetic formulation for MIN3P includes intra-aqueous and dissolution-precipitation reactions in addition to geochemical equilibrium expressions for hydrolysis, aqueous complexation, oxidation-reduction, ion exchange, surface complexation, and gas dissolution-exsolution reactions. Monod rate and inhibition terms are used to describe microbially mediated reactions or to limit the reaction progress of inorganic reactions. Mayer *et al.* (2002) present model simulations for the natural attenuation of a petroleum hydrocarbon (toluene) undergoing dissolution, volatilization, and biodegradation in an unconfined aquifer overlaid by unsaturated soils (no sorption of hydrocarbons was included). The oxidation-reduction processes simulated were primary reactions involving aerobic respiration, iron reduction (iron is sourced from amorphous and crystalline phases), and fermentation (assumed to occur simultaneously), and secondary redox reactions involving consumption of methane.

The model simulations were considered to correspond well with conditions typically observed at petroleum hydrocarbon contaminated sites (*e.g.*, Bemidji, [Baedecker *et al.*, 1993]) and provided a reasonable interpretation of natural attenuation processes. The lateral extent of the dissolved iron was only slightly (1.3 times) longer than the hydrocarbon plume. A key model process was the secondary redox reactions, which consume some of the reaction products, in particular methane and ferrous iron. For example, if the consumption of methane by ferric hydroxides were to have been excluded from the simulations, the model would have predicted high methane concentrations downgradient from the source zone into areas where the dissolved contaminant is not present. Through mass balance calculations and ^{13}C isotope analysis of methane and dissolved inorganic carbon, Amos et al. (2012) provide evidence for iron-mediated anaerobic methane oxidation at the Bemidji site.

3.3.2 Hunter *et al.* (1998)

Hunter *et al.* (1998) present model simulations for a one-dimensional, multi-component reactive transport model that accounts for the microbial degradation pathways of organic matter, as well as for secondary redox reactions and mineral precipitation–dissolution reactions. The model is used to simulate the distributions of chemical species and reaction rates for a pristine aquifer contaminated by an organic-rich leachate from a landfill. The microbial oxidation of organic matter causes the disappearance of dissolved and solid oxidants and the appearance of reduced species, but over very different spatial scales. The geochemical zonation predicted by the model was disappearance of the labile hydrocarbon fraction within first 20 m from the source, but methanogenic and iron-reducing conditions persisted to about 280 m downgradient, where there was a sharp aerobic reaction front.

3.4 Review of Field Studies

A literature review indicated that there are few documented field studies with iron and manganese data at sites with petroleum hydrocarbon or landfill leachate impacts. As stated in the BC MoE Technical Guidance 6 Working Group Report by CSAP (CSAP, 2011), the crude oil spill site at Bemidji, Minnesota has been well characterized through numerous studies (over 200 publications; Essaid *et al.*, 2011). The review below summarizes three studies that provide insight on the natural attenuation of chemical constituents associated with the crude oil spill at Bemidji. In addition, a study by Christensen *et al.* (2000) is summarized that describes the theory of redox characterization and evolution with examples from landfill leachate plumes.

3.4.1 Selected Bemidji Studies

3.4.1.1 Essaid et al. (2011)

Essaid *et al.* (2011) provide a review on long term natural attenuation and monitoring (25 years) at the Bemidji crude oil spill site. The extent and evolution of the hydrocarbon plume is shown to be the result of a complex set of processes including multiphase flow and transport, biogeochemical reactions, and microbial populations and metabolism. The review of field and modelling studies show the significance of anaerobic biodegradation reactions and in particular the role of iron reduction and methanogenesis on plume extent and longevity. The significance of the composition of the oil and differences in the evolution of the alkanes and aromatic compounds are discussed. For example, the loss of relatively soluble BTEX compounds is shown to be controlled by dissolution, which is sensitive to concentrations of these parameters in groundwater and flow rates. This review also identifies the redox zones that result from biodegradation processes in sequence of terminal electron acceptors from aerobic degradation, to manganese reduction, to iron reduction, and to methanogenesis. A summary of the modelling studies of various complexities is provided, as well as calibration of model parameters with field data.

3.4.1.2 Amos et al. (2011)

Amos *et al.* (2011) present high resolution vertical profiles of groundwater data using direct-push sampling collected in 2007 at four locations downgradient of the residual NAPL source. The data, which includes dissolved iron and manganese, is compared to historical data to assess the evolution of the plume over time. This study shows that the predominant biodegradation pathways are aerobic oxidation, manganese reduction, iron reduction, and methanogenesis. The dissolved iron plume extends from the core of the source to 120 m downgradient from the source, and corresponds to the methane plume extent. The manganese-reducing conditions, on the other hand, are identified on the fringes of the plume beyond 80 m of the source.

Using isotope analysis ($\delta^{13}C_{CH4}$), the zones of methanogenesis near the source, and microbially mediated methane oxidation downgradient from the source are identified. The high resolution data also reveals the sharp transition from the aerobic to anaerobic zone near the water table. Through measurements of N_2 concentrations near the transition zone, and multivariate and cluster analysis, the authors demonstrate the significance of gas-bubble entrapment as a transport mechanism for oxygen into the methane plume at distances closer to the source. Further downgradient from the source; however, infiltration of oxygen through mixing with recharge water is shown to be the dominant transport mechanism of oxygen into the methane plume.

3.4.1.3 Cozzarelli et al. (2001)

In this study, the monitoring of natural attenuation processes are compared on two spatial scales by analysis of pore water chemistry of data collected from water samples drained from aquifer cores (core scale), and plume scale data from observation well network. The plume scale data show that the plume lengths of iron and BTEX compounds are well correlated (*i.e.*, similar) and not changing over the study period of 1992 to 1995. However, depletion of iron oxides near the source zone is shown to result in the spread of the zone of the maximum iron concentrations. The results also show an increase in the vertical extent of the zones with maximum dissolved iron and BTEX concentrations. The authors indicate that the extent of the dissolved ferrous iron plume is controlled by processes such as microbial iron reduction and precipitation, sorption, and re-oxidation of Fe^{2+}. The core scale analysis of results near the source also show zones of concurrent iron reduction and methanogenesis.

3.4.2 Christensen *et al.* (2000)

Understanding redox conditions in the groundwater, where reducing conditions are developed from a point source of organic contamination is important for an understanding of the contaminant plume development and assessment of its natural attenuation. This review study presents the challenges of assessing the redox conditions of contaminant plumes in groundwater given slow kinetically controlled redox reactions.

Examples of assignment of redox zones are presented for municipal landfill leachates at two locations (Grindsted and Vejen). A set of criteria in terms of the concentrations of the redox sensitive parameters are used to identify zones representing methanogenic, sulfate-reducing, iron-reducing, manganese-reducing, nitrate-reducing, and aerobic conditions. For the Vejen site, the iron/manganese-reducing zone extends from a distance of 25 m to 350 m from the source. At the Grindsted landfill, four zones involving iron or manganese are identified as iron-reducing, iron/manganese-reducing, manganese-reducing, and manganese/nitrate reducing conditions. The reduced-iron and reduced-manganese concentrations extended further downgradient than the concentrations of organic compounds, as summarized by the approximate maximum downgradient extents below:

- BTEX: 70-165 m
- TVOC (total organics): 165 m
- Methane: 195 m
- Reduced iron: 230 m
- Reduced manganese: >300 m

The zone of maximum iron concentrations (100 to 150 mg/L) occurred between approximately 50 m to 105 m from the source. The zone of maximum manganese concentrations (> 25 mg/L) follows downgradient from the maximum iron concentrations from approximately 90 m to 140 m from the source. Possible reasons for a longer iron and manganese plume than TVOC plume include high source iron and manganese concentrations, low groundwater redox, the sulphide plume is limited in extent so does not have opportunity to react with iron, and non-reactive mineralogy.

Overall, the plumes at both landfill locations show the redox zones in sequence that would be expected from thermodynamic considerations; however, there are zones of overlap under reducing conditions. This is in part due to migration of redox sensitive compounds from upgradient locations (*e.g.* methane), or it may reflect concurrent redox processes (*e.g.,* iron-reduction and methanogenesis). The differences in the set of criteria used for identifying redox zones at the two landfill locations shows that the method of using redox-sensitive parameters requires knowledge of site specific conditions. The criteria depend not only on the plume composition, but also on flow velocities, soil properties and dilution, and local scale heterogeneities. The delineation of redox zones using measurements of redox-sensitive parameters also requires high spatial resolution sampling as sharp redox transition zones exist in both the vertical and horizontal directions, particularly at the fringes of the plume.

The results from the Grinsted landfill are notable in that they indicate reduced iron and manganese concentrations were highly elevated, migrated long distances, and extended well beyond the BTEX plume.

3.4.3 Roychoudhury and Merrett (2006)

A comprehensive hydro-geochemical characterization was carried out in a petroleum (gasoline)-contaminated shallow sandy aquifer in South Africa. The results indicate the presence of a BTEX plume that has moved, although only slightly, because of the flat regional hydraulic gradient. The monitoring network and flat gradient prevents a meaningful comparison of the spatial extent of BTEX and dissolved manganese and iron concentrations. However, the analysis of site mineralogy, terminal electron acceptors and metabolites provides insight on reaction processes at the site. Sulfate and iron reductions were the dominant metabolic pathways and concomitant elevated BTEX and Fe^{2+} concentrations were observed. Sulphate concentrations in the contaminated zone were depleted relative to background and, in general, sulphide concentrations were relatively low. However, in areas of higher sulphide concentrations, the Fe2+ concentrations were lower suggesting iron precipitation occurred. The dissolved manganese concentrations were similar or lower than background because solid phase manganese oxyhydroxide concentrations were limiting.

4.0 NUMERICAL MODEL DESCRIPTION

The model for this study is the three-dimensional MIN3P-DUSTY numerical model, used in two-dimensions for simulations presented herein. MIN3P-DUSTY is a finite-volume model that combines the mass conservation equations for water flow in variably-saturated porous media with multi-component reactive transport designed to simulate geochemical reactions involving solid mineral, aqueous, and gaseous species, advective-dispersive transport of dissolved species, and advective-diffusive transport of gases (Mayer *et al.*, 2002; Molins and Mayer, 2007; Molins *et al.*, 2010). In MIN3P-Dusty, the variably saturated flow module is coupled to the reactive transport module.

This numerical model provides a flexible reaction network where a number of chemical species and reaction stoichiometry's can be defined and allows for different types of rate formulations and reaction pathways. This framework is particularly useful for simulating the biodegradation of petroleum hydrocarbon compounds under aerobic and anaerobic conditions that are constrained by the availability of terminal electron acceptors (TEAs) and substrate availability. For example, the biodegradation reactions can be defined as first-order with respect to the substrate or contain a Monod type dependence, or inhibition terms, or any combination of these terms. Acid/base equilibria and mineral dissolution and precipitation reactions can also be specified, which are key processes for the fate of dissolved iron and manganese in groundwater. The model also allows for spatially and

time-varying soil moisture through water infiltration (recharge) and soil pore water transport based on the solution to Richards equation. The transport of the gas phase includes an advective component and the Dusty Gas model (DGM) for simulation of multicomponent gas diffusion. A detailed description of the model is provided in Mayer *et al.* (2002) and Molins and Mayer (2007).

The application of the MIN3P-Dusty code for this study implements all of the key model processes described in Section 3.0 of this report, consisting of advective-dispersive transport of groundwater, dissolution of hydrocarbon compounds from LNAPL, dissolution and precipitation of mineral components, primary and secondary redox reactions, aqueous complexation and absorption of petroleum hydrocarbon compounds.

Oxidation-reduction reactions for nitrate and sulphate are not included because of limited kinetic data for these parameters. Lack of inclusion of these reactions is not likely to have a significant effect on the results because natural attenuation studies have shown that the combined assimilative capacity of TEAs considered in the modeling (oxygen, iron, manganese and carbon dioxide) is much higher than that of nitrate and sulphate. For example, U.S. EPA (1998) report, on average, the measured TEAs for oxygen, iron, manganese and carbon dioxide for multiple field sites comprised 80% of the assimilative capacity. However, there can be elevated sulphate concentrations in groundwater in the Lower Mainland region, especially in areas close to the coast, and therefore, sulphate reduction and associated secondary redox reactions, such as iron sulphide precipitation may be significant. Sorption of dissolved iron and manganese is not included given the uncertainty in sorption rates, consistent with modeling studies by Hunter *et al.* (1998) and Mayer *et al.* (2002).

5.0 MODEL SIMULATION SETUP AND INPUT PARAMETERS

The MIN3P-Dusty numerical model was set up to simulate the natural attenuation of petroleum hydrocarbon compounds through dissolution, volatilization and biodegradation and transport of iron and manganese. The model setup follows the description in the conceptual site model in that a residual phase gasoline hydrocarbon source at the water table is simulated. The residual phase source hydrocarbon is 1.0 m wide, 20 m long (in direction of groundwater flow) and one metre thick.

For purposes of describing physical-chemical properties, the gasoline contamination is assumed to be solely comprised of benzene. This approximation is considered reasonable because dissolved plumes in groundwater at gasoline release sites are comprised primarily of aromatic hydrocarbons with similar properties to benzene. The hydrocarbon contamination is present in an otherwise pristine (oxic conditions) background soil. The following sections define the input parameters for hydrogeologic and geochemical conditions.

5.1 Model Domain and Soil Properties

The model is set up in two-dimensions (x and z) with the LNAPL source zone located near one end of a 600 m by 15 m solution domain (Figure 2). The water table is located at approximately 3 m below ground surface. The hypothetical problem formulation is based on the release of petroleum hydrocarbons in the vadose zone that would result in residual-phase product with relatively low saturation (S_o = 1%) in the vadose zone and a higher saturation in the capillary fringe (S_o = 10%). The zone with the residual phase product in the vadose zone is assumed to be 10 m long and 2.0 m thick, while the higher saturation zone in the capillary fringe is assumed to be 20 m long and 1.0 m thick. The hydrocarbon components are assumed to dissolve and biodegrade under aerobic and anaerobic conditions both in the saturated and unsaturated soil zones. Volatilization of hydrocarbons occurs at the top of the capillary fringe.

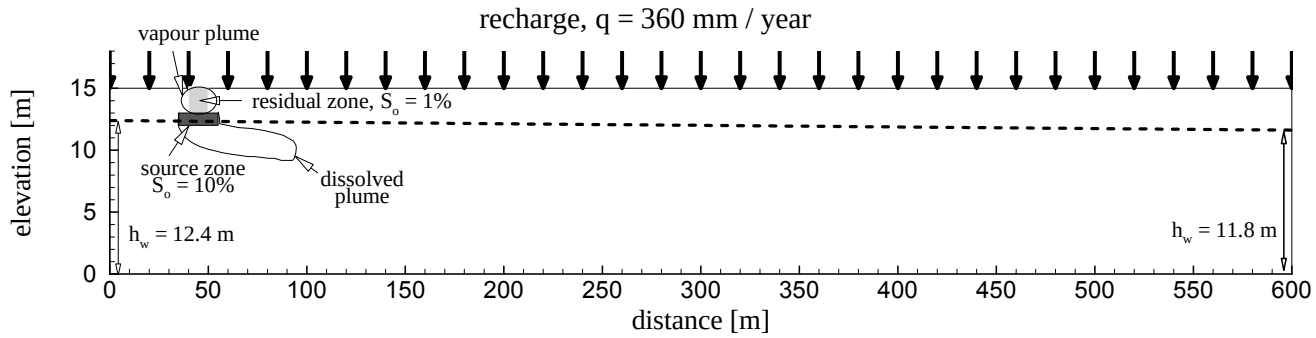

Figure 2: Model domain with location of petroleum hydrocarbon LNAPL with saturation, S_o = 1% in the unsaturated zone and S_o = 10% in the source zone.

The soil properties and hydrogeological conditions are selected based on a literature search to obtain parameter values representative of "typical" conditions in the Lower Mainland region of British Columbia (near Vancouver). The model domain is assumed to be a vertical cross-section in the direction of the groundwater flow with thickness of 15 m and horizontal distance of 600 m. The soil is assumed to consist of a 3 m layer of silty sand from ground surface overlying Fraser River sand. Table 2 summarizes the soil and hydrogeological parameters input to the model.

Table 2: Soil physical properties.

Parameter	Unit	Fraser River Sand	Silty Sand
Porosity, ϕ	-	0.38	0.39
Soil hydraulic function (Van Genuchten) parameters: α	1/m	3.5	2.7
N	-	3.2	1.4
Residual water saturation, S_r	-	0.053	0.039
Temperature	°C	10	10
Specific storage coefficient	1/m	1.8×10^{-4}	1.0×10^{-4}
Saturated hydraulic conductivity: $K_{xx} = K_{zz}$	m/s	5.2×10^{-4}	6.0×10^{-5}
Hydraulic head gradient	m/m	1.0×10^{-3}	-
Longitudinal dispersivity	m	1.0	0
Transverse dispersivity	m	0.01	0
Recharge rate	m/yr	-	0.36

The porosity and soil hydraulic function parameters are based on generic values for sand and sandy loam, which is assumed to approximate the silty sand (Tillman and Weaver, 2007). The specific storage coefficient and hydraulic conductivity of the silty sand layer are taken from the study of Neilson-Welch and Smith (2001) for similar soil (Unit 2 in that study). The temperature in the soil is assumed to be the average air temperature of the region and is the average recorded temperature at the Environment Canada Vancouver International Airport weather station from 1971-2000.

The specific storage coefficient, hydraulic conductivity and the hydraulic head gradient for the Fraser River sand layer are based on the Zawadzki *et al.* (2002) study at a site on the north side of the Fraser River estuary and approximately 20 km upstream from the Pacific Ocean. These selected values for Fraser River sand are similar to those obtained in other studies. For example, Neilson-Welch and Smith (2001) estimate hydraulic conductivity of 4 x 10^{-4} m/s for the sand layers at a site in Richmond, BC, and Jackson *et al.* (2006) select values of 2.1 x 10^{-4} m/s for the sand aquifer at a site along the lower Fraser River near Vancouver, BC.

Each layer in the model domain is assumed to represent isotropic and homogeneous soil conditions. The longitudinal and transverse dispersivity are assumed to be 1.0 m and 0.01 m, respectively (Neilson-Welch and Smith, 2001; Schulze-Makuch, 2005) for the Fraser River sand layer. The recharge rate is estimated from an average annual precipitation (Vancouver International Airport) of 1060 mm and evapotranspiration of 490 mm (Valentine *et al.*, 1978) and assuming 20% run-off.

5.2 Variably Saturated Flow Module

The steady state solution to the flow module is used to define the moisture distribution and the Darcy velocity field for the aqueous phase in the model domain. The boundary conditions are defined by constant recharge of 360 mm/year at the upper boundary (z = 15 m) and a constant hydraulic gradient of 0.001 m/m across the domain as described in Table 2. The water table is assumed to be at a depth of approximately 3 m below ground surface (at z = 12.4 m (x = 0) and at z = 11.8 m (x = 600 m)).

The porosity is reduced in the residual hydrocarbon source zone and the vadose residual zone to account for the presence (volume) of the hydrocarbon. Similarly, the permeability of the residual hydrocarbon source zone and vadose residual zone is reduced by 80% and 25%, respectively (Mayer *et al.*, 2002). However, the porosity and permeability fields are assumed to be constant in time and are not adjusted as the source is depleted.

5.3 Reactive Transport Module

The dissolution, volatilization, and biodegradation of the hydrocarbon component (represented by benzene in this study) derive the geochemical transformations in the soil and groundwater. Dissolution and volatilization are described as reversible reactions based on the solubility and the Henry's constant, respectively. The hydrocarbon component in liquid form is defined as a mineral $C_6H_{6(l)}$ that dissolves into the aqueous phase $C_6H_{6(aq)}$ and is in equilibrium with the gas phase $C_6H_{6(g)}$.

Aerobic and anaerobic biodegradation reactions are assumed to occur in the aqueous phase. The biodegradation reactions involve oxygen (O_2), manganese (IV) mineral (MnO_2), and iron (III) minerals ($Fe(OH)_3$ and FeO(OH)), as well as fermentation resulting in the production of methane (CH_4). Denitrification and sulphate reduction are not included as primary redox reactions assuming absence of nitrate and sulphate in the background groundwater.

The transport processes are considered to be advective flow (Darcy's law) for the aqueous phase with the Darcy velocity field as derived from the steady state solution of the variably saturated flow module. Dispersion and molecular diffusion are also considered for the aqueous phase, while only molecular diffusion is considered for the gas phase. A single diffusion coefficient is assumed for all chemical species that is 2 x 10^{-5} m^2/s in the gas phase and 8 x 10^{-10} m^2/s in the aqueous phase.

5.3.1 Chemical Species & Reaction Network

In MIN3P-Dusty, the mass balance equations are solved for the dissolved aqueous species termed total component concentrations. The total component concentrations are related to the individual aqueous complexes and the gas phase by assuming equilibrium conditions (*e.g.*, the gas phase concentration of a component is assumed to be related to its aqueous concentration through Henry's law). Mass balance is also considered for the mineral species, including the LNAPL phase, which are coupled to the components through specified kinetic reaction rates describing mineral dissolution or precipitation.

The reaction network for this study consists of the reduction-oxidation (redox) reactions for the degradation of benzene (primary redox reactions) and the re-oxidation reactions of the produced Fe^{2+}, Mn^{2+}, and CH_4 (secondary redox reactions) as summarized in Table 3. The primary and secondary redox reactions result in the production and consumption of protons, which alter the pH and the saturation index of the minerals. Therefore, the related aqueous complexation reactions and mineral dissolution and precipitation of calcite, siderite, and rhodochrosite are also included. Linear sorption is also considered for benzene with partitioning coefficient, K_{oc}, equal to 58.9 cm^3/g (US EPA, 2004) and fraction organic carbon, f_{oc}, equal to 0.006 (SABCS, 2010).

Table 3: Reaction network.

Primary redox reactions for benzene:	
R_{pr1}	$C_6H_6 + 7.5O_2 + 3H_2O \rightarrow 6CO_3^{2-} + 12H^+$
R_{pr2}	$\frac{1}{15}C_6H_6 + MnO_2 + \frac{6}{5}H^+ \rightarrow Mn^{2+} + \frac{2}{5}CO_3^{2-} + \frac{4}{5}H_2O$
R_{pr3}	$\frac{1}{30}C_6H_6 + FeOOH + \frac{8}{5}H^+ \rightarrow Fe^{2+} + \frac{1}{5}CO_3^{2-} + \frac{7}{5}H_2O$
R_{pr4}	$\frac{1}{30}C_6H_6 + Fe(OH)_3 + \frac{8}{5}H^+ \rightarrow Fe^{2+} + \frac{1}{5}CO_3^{2-} + \frac{12}{5}H_2O$
R_{pr5}	$C_6H_6 + \frac{27}{4}H_2O \rightarrow \frac{9}{4}CO_3^{2-} + \frac{9}{2}H^+ + \frac{15}{4}CH_4$
Secondary redox reactions:	
R_{sr1}	$CH_4 + 2O_2 \rightarrow CO_3^{2-} + 2H^+ + H_2O$
R_{sr2}	$Fe^{2+} + \frac{1}{4}O_2 + H^+ \rightarrow Fe^{3+} + \frac{1}{2}H_2O$
R_{sr3}	$Mn^{2+} + \frac{1}{2}O_2 + H_2O \rightarrow MnO_2 + 2H^+$
R_{sr4}	$2Fe^{2+} + MnO_2 + 4H^+ \rightarrow 2Fe^{3+} + Mn^{2+} + 2H_2O$
R_{sr5}	$\frac{1}{4}CH_4 + MnO_2 + \frac{3}{2}H^+ \rightarrow Mn^{2+} + \frac{1}{4}CO_3^{2-} + \frac{5}{4}H_2O$
R_{sr6}	$\frac{1}{8}CH_4 + FeO(OH) + \frac{7}{4}H^+ \rightarrow Fe^{2+} + \frac{1}{8}CO_3^{2-} + \frac{13}{8}H_2O$
R_{sr7}	$\frac{1}{8}CH_4 + Fe(OH)_3 + \frac{7}{4}H^+ \rightarrow Fe^{2+} + \frac{1}{8}CO_3^{2-} + \frac{21}{8}H_2O$

Mineral dissolution / precipitation reactions (non-redox):			
R_{m1}	$CaCO_3 \leftrightarrow Ca^{2+} + CO_3^{2-}$		
R_{m2}	$FeCO_3 \leftrightarrow Fe^{2+} + CO_3^{2-}$		
R_{m3}	$MnCO_3 \leftrightarrow Mn^{2+} + CO_3^{2-}$		
R_{m4}	$C_6H_{6(l)} \leftrightarrow C_6H_{6(aq)}$		
R_{m5}	$Fe(OH)_3 + 3H^+ \leftrightarrow Fe^{3+} + 3H_2O$		
R_{m6}	$MnO_2 \leftrightarrow MnO_{2(aq)}$		
Aqueous complexation reactions:			
R_{c1}	$Fe(OH)^+ + H^+ \leftrightarrow Fe^{2+} + H_2O$	R_{c12}	$OH^- + H^+ \leftrightarrow H_2O$
R_{c2}	$Fe(OH)_3^- + 3H^+ \leftrightarrow Fe^{2+} + 3H_2O$	R_{c13}	$HCO_3^- \leftrightarrow CO_3^{2-} + H^+$
R_{c3}	$FeHCO_3^+ \leftrightarrow Fe^{2+} + CO_3^{2-} + H^+$	R_{c14}	$H_2CO_{3(aq)} \leftrightarrow CO_3^{2-} + 2H^+$
R_{c4}	$FeCO_{3(aq)} \leftrightarrow Fe^{2+} + CO_3^{2-}$	R_{c15}	$Ca(OH)^+ + H^+ \leftrightarrow H_2O + Ca^{2+}$
R_{c5}	$Fe(OH)_2 + 2H^+ \leftrightarrow Fe^{2+} + 2H_2O$	R_{c16}	$CaHCO_3^+ \leftrightarrow CO_3^{2-} + Ca^{2+} + H^+$
R_{c6}	$Fe(OH)^{2+} + H^+ \leftrightarrow Fe^{3+} + H_2O$	R_{c17}	$CaCO_{3(aq)} \leftrightarrow CO_3^{2-} + Ca^{2+}$
R_{c7}	$Fe(OH)_2^+ + 2H^+ \leftrightarrow Fe^{3+} + 2H_2O$	R_{c18}	$MnCO_{3(aq)} \leftrightarrow CO_3^{2-} + Mn^{2+}$
R_{c8}	$Fe(OH)_3 + 3H^+ \leftrightarrow Fe^{3+} + 3H_2O$	R_{c19}	$MnHCO_3^+ \leftrightarrow CO_3^{2-} + Ca^{2+} + H^+$
R_{c9}	$Fe(OH)_4^- + 4H^+ \leftrightarrow Fe^{3+} + 4H_2O$	R_{c20}	$Mn(OH)^+ + H^+ \leftrightarrow Mn^{2+} + H_2O$
R_{c10}	$Fe_2(OH)_2^{4+} + 42 \leftrightarrow 2Fe^{3+} + 2H_2O$	R_{c21}	$Mn(OH)_3^- + 3H^+ \leftrightarrow Mn^{2+} + 3H_2O$
R_{c11}	$Fe_3(OH)_4^{5+} + 4H^+ \leftrightarrow 3Fe^{3+} + 4H_2O$		
Gas dissolution / exsolution reactions:			
R_{g1}	$C_6H_{6(g)} \leftrightarrow C_6H_{6(aq)}$		
R_{g2}	$O_{2(g)} \leftrightarrow O_{2(aq)}$		
R_{g3}	$CO_{2(g)} + H_2O \leftrightarrow CO_3^{2-} + 2H^+$		
R_{g4}	$CH_{4(g)} \leftrightarrow CH_{4(aq)}$		

Given the reaction network as summarized in Table 3, ten components are considered in this study: C_6H_6, O_2, CO_3^{2-}, H^+, $CH_{4(aq)}$, Fe^{2+}, Ca^{2+}, Mn^{2+}, $MnO_{2(aq)}$, and Fe^{3+}. The gaseous species are $C_6H_{6(g)}$, $O_{2(g)}$, $CO_{2(g)}$, and $CH_{4(g)}$. There are also seven minerals that participate in the mineral dissolution and precipitation reactions: $C_6H_{6(l)}$, MnO_2, $Fe(OH)_3$, $FeO(OH)$, $CaCO_3$, $MnCO_3$, and $FeCO_3$.

5.3.2 Reaction Rate Formulations

The reactions summarized in Table 3 can be described by kinetic rates, where the rates are slow on the timescale of transport processes. These include the irreversible primary and secondary redox reactions and the reversible mineral dissolution and precipitation reactions. All other reactions are described by equilibrium conditions. Table 4 summarizes the rate formulations for the kinetic reactions and equilibrium constants used to describe the reaction network. The effective solubility of $C_6H_{6(l)}$ is assumed to be 100 mg/L, representing a conservatively high value for benzene, but within the lower range for total petroleum hydrocarbon concentrations as compiled in the US EPA Petroleum Vapor Intrusion Database (January 2013) for LNAPL sources and mostly gasoline releases.

Table 4: Reaction rate formulations and equilibrium constants[1].

Formula	Parameters	Sources
Primary redox reactions for benzene:		
$R_{pr1} = k_{pr1}[C_6H_6]\frac{[O_2]}{[O_2]+K_{mp1}}$	$k_{pr1} = 0.02\ day^{-1}$ $K_{mp1} = 3.1\times10^{-6} mol/L$	Morasch et al. (2011) Mayer et al. (2002)
$R_{pr2} = k_{pr2}\frac{[C_6H_6]}{[C_6H_6]+K_{mp2\_1}}\frac{[MnO_2]}{[MnO_2]+K_{mp2\_2}}\frac{K_{ip2\_1}}{[O_2]+K_{ip2\_1}}$	$k_{pr2} = 2.4\times10^{-13} mol/L_{bulk}/s$ $K_{mp2\_1} = 1.1\times10^{-6} mol/L$ $K_{mp2\_2} = 10^{-7}$ $K_{ip2\_1} = 3.1\times10^{-6} mol/L$	Molins et al. (2010) Added Monod term for MnO_2
$R_{pr3} = k_{pr3}\frac{[C_6H_6]}{[C_6H_6]+K_{mp3\_1}}\frac{[FeO(OH)]}{[FeO(OH)]+K_{mp3\_2}}\frac{K_{ip3\_1}}{[O_2]+K_{ip3\_1}}$	$k_{pr3} = 2.4\times10^{-13} mol/L_{bulk}/s$ $K_{mp3\_1} = 2.5\times10^{-4} mol/L$ $K_{mp3\_2} = 10^{-7}$ $K_{ip3\_1} = 3.1\times10^{-6} mol/L$	Mayer et al. (2002) Added Monod term for FeO(OH)
$R_{pr4} = k_{pr4}\frac{[C_6H_6]}{[C_6H_6]+K_{mp4\_1}}\frac{[Fe(OH)_3]}{[Fe(OH)_3]+K_{mp4\_2}}\frac{K_{ip4\_1}}{[O_2]+K_{ip4\_1}}$	$k_{pr4} = 1.2\times10^{-12} mol/L_{bulk}/s$ $K_{mp4\_1} = 5.0\times10^{-5} mol/L$ $K_{mp4\_2} = 10^{-7}$ $K_{ip4\_1} = 3.1\times10^{-6} mol/L$	Mayer et al. (2002) Added Monod term for $Fe(OH)_3$
$R_{pr5} = k_{pr5}\frac{[C_6H_6]}{[C_6H_6]+K_{mp5\_1}}\frac{K_{ip5\_1}}{[O_2]+K_{ip5\_1}}$	$k_{pr5} = 2.5\times10^{-12} mol/L/s$ $K_{mp5\_1} = 1.0\times10^{-4} mol/L$ $K_{ip5\_1} = 3.1\times10^{-5} mol/L$	Mayer et al. (2002)
Secondary redox reactions:		
$R_{sr1} = k_{sr1}\frac{[O_2]}{[O_2]+K_{ms1\_1}}\frac{[CH_4]}{[CH_4]+K_{ms1\_2}}$	$k_{sr1} = 1.0\times10^{-9} mol/L/s$ $K_{ms1\_1} = 3.1\times10^{-6} mol/L$ $K_{ms1\_2} = 1.0\times10^{-5} mol/L$	Mayer et al. (2002)
$R_{sr2} = k_{sr2}\frac{[O_2]}{[O_2]+K_{ms2\_1}}\frac{[Fe^{2+}]}{[Fe^{2+}]+K_{ms2\_2}}\frac{K_{is2\_1}}{[CH_4]+K_{is2\_1}}\frac{K_{is2\_2}}{[C_6H_6]+K_{is2\_2}}$	$k_{sr2} = 1.0\times10^{-8} mol/L/s$ $K_{ms2\_1} = 3.1\times10^{-6} mol/L$ $K_{ms2\_2} = 1.0\times10^{-5} mol/L$ $K_{is2\_1} = 1.0\times10^{-7} mol/L$ $K_{is2\_2} = 1.0\times10^{-7} mol/L$	Mayer et al. (2002)
$R_{sr3} = k_{sr3}\frac{[O_2]}{[O_2]+K_{ms3\_1}}\frac{[Mn^{2+}]}{[Mn^{2+}]+K_{ms3\_2}}\frac{K_{is3\_1}}{[CH_4]+K_{is3\_1}}\frac{K_{is3\_2}}{[C_6H_6]+K_{is3\_2}}$	$k_{sr3} = 5.0\times10^{-9} mol/L/s$ $K_{ms3\_1} = 3.1\times10^{-6} mol/L$ $K_{ms3\_2} = 1.0\times10^{-5} mol/L$ $K_{is3\_1} = 1.0\times10^{-7} mol/L$ $K_{is3\_2} = 1.0\times10^{-7} mol/L$	Based on same O_2 consumption rate as R_{sr2}
$R_{sr4} = k_{sr4}[Fe^{2+}][MnO_2]$	$k_{sr4} = 0.0 M^{-1}yr^{-1}$ $k_{sr4} = 1.0\times10^{3} M^{-1}yr^{-1}$	See text
$R_{sr5} = k_{sr5}\frac{[CH_4]}{[CH_4]+K_{ms5\_1}}\frac{[MnO_2]}{[MnO_2]+K_{ms5\_2}}\frac{K_{is5\_1}}{[O_2]+K_{is5\_1}}$	$k_{sr5} = 10^{-12} mol/L_{bulk}/s$ $K_{ms5\_1} = 5.0\times10^{-3} mol/L$ $K_{ms5\_2} = 10^{-7}$ $K_{is5\_1} = 3.1\times10^{-6} mol/L$	Mayer et al. (2002)
$R_{sr6} = k_{sr6}\frac{[CH_4]}{[CH_4]+K_{ms6\_1}}\frac{[FeO(OH)]}{[FeO(OH)]+K_{ms6\_2}}\frac{K_{is6\_1}}{[O_2]+K_{is6\_1}}$	$k_{sr6} = 10^{-12} mol/L_{bulk}/s$ $K_{ms6\_1} = 5.0\times10^{-3} mol/L$ $K_{ms6\_2} = 10^{-7}$ $K_{is6\_1} = 3.1\times10^{-6} mol/L$	Mayer et al. (2002)
$R_{sr7} = k_{sr7}\frac{[CH_4]}{[CH_4]+K_{ms7\_1}}\frac{[Fe(OH)_3]}{[Fe(OH)_3]+K_{ms7\_2}}\frac{K_{is7\_1}}{[O_2]+K_{is7\_1}}$	$k_{sr7} = 5.0\times10^{-12} mol/L_{bulk}/s$ $K_{ms7\_1} = 1.0\times10^{-3} mol/L$ $K_{ms7\_2} = 10^{-7}$ $K_{is7\_1} = 3.1\times10^{-6} mol/L$	Mayer et al. (2002)

[1] Note that the solubilities and equilibrium constants reflect values at standard temperature. The enthalpy change of reaction is used to compute constants at 10.1 °C.

Mineral dissolution / precipitation reactions (non-redox): $R_m = k_m\left(1 - \frac{IAP}{K_s}\right)$			
Rate	*k_m (mol/L_{bulk}/s)*	*pK_s*	*Sources*
R_{m1}	1.0×10^{-9}	8.475	Mayer et al. (2002)
R_{m2}	1.0×10^{-20}	10.89	Mayer et al. (2002)
R_{m3}	1.0×10^{-20}	10.41	Mayer et al. (2002)
R_{m4}	1.0×10^{-7}	2.336	Mayer et al. (2002)
R_{m5}	1.0×10^{-11}	-2.891	Mayer et al. (2002)
R_{m6}	1.0×10^{-15}	15.0	Molins et al. (2010) – assuming nearly insoluble
Aqueous complexation reactions: Equilibrium constant K			
Reaction	*pK*	*Reaction*	*pK*
R_{c1}	*-9.50*	R_{c12}	-14.0
R_{c2}	*-31.0*	R_{c13}	10.3
R_{c3}	12.3	R_{c14}	16.7
R_{c4}	4.38	R_{c15}	-12.8
R_{c5}	-20.6	R_{c16}	11.4
R_{c6}	-2.19	R_{c17}	3.22
R_{c7}	-5.67	R_{c18}	4.90
R_{c8}	-12.6	R_{c19}	12.3
R_{c9}	-21.6	R_{c20}	-10.6
R_{c10}	-2.95	R_{c21}	-34.8
R_{c11}	*-6.30*		
Gas dissolution / exsolution reactions: Henry's constant, K_H (atm L/mol)			
Reaction	*Log(K_H)*		
R_{g1}	*0.748*		
R_{g2}	2.90		
R_{g3}	18.16		
R_{g4}	2.89		

There are a wide range of values reported for the first-order biodegradation rate constant of benzene or BTEX compounds for groundwater plumes. For example, ASTM (2004) report a biodegradation rate range of 0.001 to 0.01 day^{-1} for BTEX, citing the study of Salanitro (1993). Essaid *et al.* (2003) estimate a rate constant that is approximately an order of magnitude higher (0.15 day^{-1}) based on inverse modelling of a BTEX plume from a crude-oil spill site (Bemidji, MN). In a microcosm study, Morasch *et al.* (2011) report a rate of 0.021 day^{-1} for benzene biodegradation through compound specific isotope analysis (CSIA) of ^{13}C-benzene for sediments (and groundwater) from the unsaturated zone that is exposed to air. For the aerobic biodegradation rate in this study, we assume a first-order rate constant of 0.02 day^{-1} that is in line with the study of Morash *et al.* (2011) for benzene, and is within the range of reported values for BTEX.

The rate of Fe^{2+} oxidation by reductive dissolution of MnO_2 is set to zero for the simulations presented in this report. There is a high degree of uncertainty in the rate constant for this reaction, which impacts the distribution of dissolved Fe^{2+}. In the database prepared by Katsev *et al.* (2004), the range of values for this reaction derived from the literature is 1.0 x 10^3 M^{-1} yr^{-1} to 1.0 x 10^6 M^{-1} yr^{-1}. In a groundwater modelling study, Hunter *et al.* (1998) assume a rate of 1.0 x 10^3 M^{-1} yr^{-1} and report a range of less than 10^9 M^{-1} yr^{-1} from the literature. In both studies, the rate formulation is assumed to be bimolecular and independent of pH, which could have a significant effect on the rates. Therefore, further investigation on the effect and formulation of this reaction is required that is beyond the scope of this project.

5.3.3 Initial Conditions

Two rectangular source zones are defined for the residual hydrocarbon similar to the hypothetical case simulated in Mayer *et al.* (2002): 1) residual LNAPL saturation at 1% extending over a length of 10 m in the vadose zone; and 2) a 1 m thick zone with saturation of 10% extending over a length of 20 m at the water table. The rest of the model domain is assumed to be initially free of hydrocarbon contaminants, and nitrate and sulphate, as well as dissolved iron and manganese concentrations are initially zero throughout the domain. The initial conditions for component concentrations and volume fractions of the minerals are summarized in Table 5.

Table 5: Initial chemical composition of the model domain.

Component	**Entire domain**		
Ca^{2+} (mol/L)	7.0 x 10^{-4}		
Fe_{tot} (mol/L)	2.8 x 10^{-9}		
pCO_2 (ppm)	380		
pO_2 (atm)	0.21		
pH	8.2		
Mineral Volume Fractions			
Calcite[a]	1%		
Ferrihydrite	0.025%		
Goethite	0.25%		
MnO_2	0.05%		
Siderite	0		
Rhodochrosite	0		
$C_6H_{6(l)}$	**Background**	**Residual hydrocarbon zone at water table**	**Residual hydrocarbon zone in vadose zone**
	0	10%	1%

[a]Value is the same as in the modelling study of Molins *et al.* (2010) for a crude oil spill at Bemidji.

The initial chemical composition for the aqueous and gas phase is based on equilibration of rainwater chemistry with ferrihydrite and calcite. The assumed rainwater chemistry is described in boundary conditions section below. The iron mineral content is assumed to consist of crystalline and amorphous phases represented by goethite and ferrihydrite, respectively following the example of Mayer *et al.* (2002) and using the same ratio. The volume fractions of goethite and manganese dioxide were increased by an order of magnitude compared to those reported in Molins *et al.* (2010) based on available local data (Table 6).

Table 6: Iron and manganese mineral content.

Mineral Type	Volume Fraction	Source	Notes
FeO(OH)	2.5×10^{-4}	Molins *et al.* (2010)	Modelling study of crude oil spill at Bemidji, MN
FeO(OH)	1.0×10^{-5}	Mayer *et al.* (2002)	Modelling study of hypothetical scenario simulating hydrocarbon degradation
FeO(OH)	$8.8 \times 10^{-4} – 1.9 \times 10^{-3}$	Mark Bolton Thesis 2004	DND and Kidd2 sediment cores and sequential extraction procedure [a]
FeO(OH)	$2.1 \times 10^{-2} – 2.7 \times 10^{-2}$	Golder (2005)	Fraser River Sand XRF data from trace rock chemistry [b]
$Fe(OH)_3$	1.0×10^{-6}	Mayer *et al.* (2002)	Modelling study of hypothetical scenario simulating hydrocarbon degradation
$Fe(OH)_3$	$1.3 \times 10^{-3} – 3.1 \times 10^{-3}$	Mark Bolton Thesis 2004	DND and Kidd2 sediment cores and sequential extraction procedure [c]
MnO_2	5×10^{-5}	Molins *et al.* (2010)	Modelling study of crude oil spill at Bemidji, MN
MnO_2	$3.9 \times 10^{-4} – 4.6 \times 10^{-4}$	Golder (2005)	Fraser River Sand XRF data from trace rock chemistry [d]
Fe_2O_3	3.0×10^{-3}	Anett Briggs (Golder Associates, pers. Comm. October 5, 2012)	Roberts Bank sediment XRD data
Fe_2O_3	1.9×10^{-2}	Golder (2005)	Fraser River Sand XRF data from whole rock analysis
Fe_3O_4	$1.5 \times 10^{-3} – 2.0 \times 10^{-3}$	Anett Briggs (pers. Comm. October 5, 2012)	Roberts Bank sediment XRD data

[a] It is assumed that goethite represents the target phase of crystalline Fe oxyhydroxides reported.
[b] It is assumed that the reported trace Fe is associated with goethite.
[c] It is assumed that ferrihydrite represents the target phase of amorphous Fe oxyhydroxides reported.
[d] It is assumed that the reported trace Mn is associated with manganese dioxide.

5.3.4 Boundary Conditions

The boundary conditions are defined by a constant recharge at the top boundary at z = 15 m. The chemical composition of the recharge water and the background groundwater are summarized in Table 7. The recharge water composition is based on rainwater composition reported by Mayer *et al.* (2002). However, the pH and pCO_2 have been adjusted to 5.9 ppm and 380 ppm (at standard temperature), respectively. The background groundwater chemistry is based on the rainwater equilibration with ferrihydrite, calcite and manganese oxide assuming an open system to the atmosphere.

Table 7: Chemical composition of recharge water and background groundwater.

Component	Recharge Water	Background Groundwater
Ca^{2+} (mol/L)	2.5×10^{-6}	7.0×10^{-4}
Fe_{tot} (mol/L)	-	2.8×10^{-9}
pCO_2 (ppm)	380	380
pO_2 (atm)	0.21	0.21
pH	5.9	8.2

6.0 MODEL SIMULATION RESULTS

Four scenarios of a hydrocarbon spill and its fate and transport in the subsurface based on the model definition described in Section 5.0 were simulated. The input parameters as described above define the baseline Scenario 1. Alternative realizations of the model were based on variations of key input parameters to assess the model under differing geochemical and hydrological conditions. The results of simulations for four scenarios are presented, as follows:

- Scenario 1, baseline;
- Scenario 2, reduced flow rates;
- Scenario 3, hydrocarbon source depletion represented by a thinner hydrocarbon layer at the capillary fringe;
- Scenario 4, hydrocarbon source removal after 10 years;
- Scenario 5, methane generation from anaerobic degradation of benzene is set to zero; and
- Scenario 6, three dimensional simulation (all others are two dimensional).

The assumptions for the different scenarios are described below.

Steady state conditions were assumed for the flow module, and the transient reactive transport module was run over a time period of 20 years (except for Scenario 3 that was simulated to 50 years) with a maximum time step of 0.1 years.

6.1 Steady state results of variably saturated flow

The first step in the modeling process was to run the variably saturated flow module. The steady state solutions of this flow model are shown in Figure 3 and 4 as well as the input porosity field. Lower porosities and permeabilities are assumed in the source and residual zones. The hydraulic head and water saturation are used to compute the Darcy flow velocities for the aqueous phase.

For Scenarios 1, 3 and 4, the input parameters in Table 2 were used for the modeling. The predicted Darcy velocity is 16 m/year and the groundwater velocity is 44 m/year, both at the middle of the domain (x = 300 m).

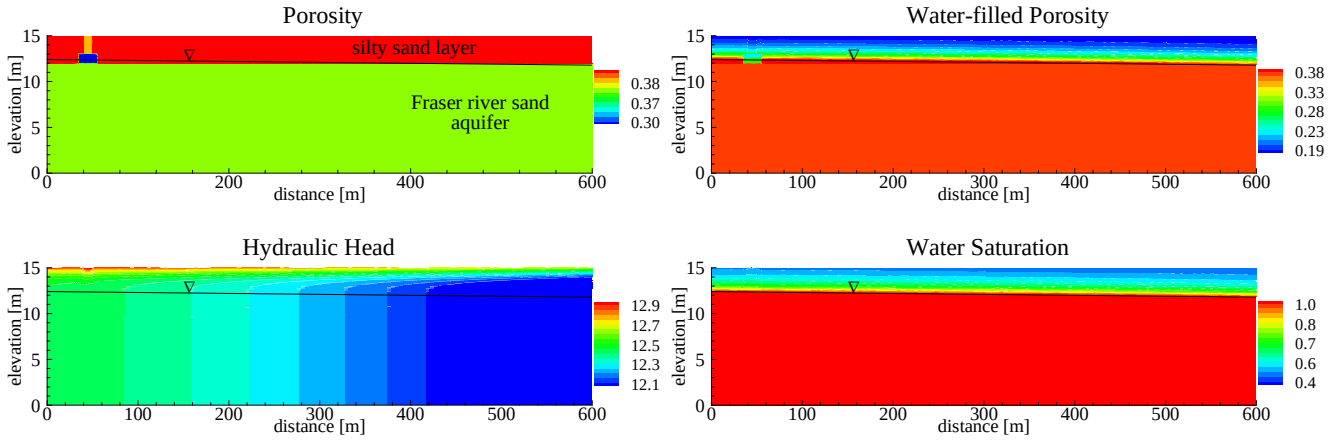

Figure 3: Input porosity field and the steady state flow results for variably saturated flow for Scenarios 1, 3 and 4.

Reduced flow rates were assumed in Scenario 2 to evaluate its effect on the separation distance between the hydrocarbon plume and the dissolved Fe^{2+} and Mn^{2+} plumes. Three input parameters were changed to reduce the flow rates:

1) The recharge rate was reduced from 360 mm/year to 200 mm/year.

2) The hydraulic conductivity of the aquifer was reduced by 10 times from 5.2 x 10^{-4} m/s to 5.0 x 10^{-5} m/s.

3) The hydraulic gradient was increased to 0.00375 m/m from 0.001 m/m.

The Scenario 2 assumptions for the above parameters are consistent with Mayer *et al.* (2002). The reason for choosing parameters consistent with Mayer *et al.* (2002) is to enable comparisons to reactive transport modeling in that paper. The depth to the water table and porosity were kept the same as in the baseline Scenario 1.

The steady state results of the flow model for this Scenario are shown in Figure 4. The predicted Darcy velocity for Scenario 2 at the middle of domain (x = 200 m) is 5.8 m/year and the groundwater velocity is 16 m/year.

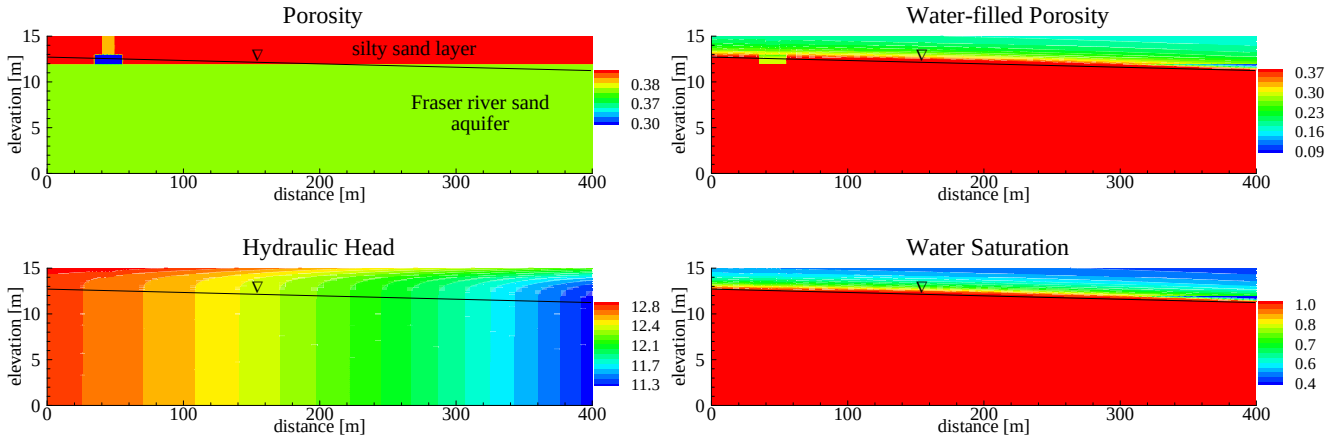

Figure 4: Input porosity field and the steady state flow results for variably saturated flow for Scenario 2.

6.2 Reactive Transport Model Results

The MIN3P-Dusty reactive transport model is used to simulate six Scenarios with the baseline Scenario 1 representing the model input parameters defined in Section 5. The baseline Scenario 1 represents a specific set of hydrological and geochemical conditions, on which the predicted results are based. Therefore, to assess the effect of select input parameters and the effect of dimensionality, five additional scenarios are defined in the following sections. The results present relative plume lengths and distribution of the hydrocarbon (benzene) and the dissolved iron and manganese concentrations, as well as the plume longevity following the depletion or removal of the residual-phase hydrocarbon source.

6.2.1 Baseline Scenario 1

The results of the baseline simulation (Scenario 1) at 10 years simulation time are summarized in Figure 5. The hydrocarbon plume length is approximately 120 m (defined as a concentration greater than 5 mg/L), with a zone of high benzene concentrations in the residual hydrocarbon source zone, but much lower concentrations downgradient of the source due to natural attenuation. As expected, the hydrocarbon biodegradation reactions result in the production of methane, Fe^{2+}, and Mn^{2+}, and the depletion of oxygen. The plume length for the reduced Fe^{2+} and Mn^{2+} species is approximately 390 m, or about 270 m longer than that of the hydrocarbon plume. The methane plume follows the same approximate trend and is only approximately 20 m shorter than the Fe^{2+} and Mn^{2+} plumes.

In addition to the difference in plume length, the highest concentrations of CH_4, Fe^{2+} and Mn^{2+} are located near the centre of the plume. The parameters affected at the farthest distance from the contamination source are O_2, CO_2, and pH as shown in Figure 5. Based on the average groundwater velocity of 44 m/year, the plume is expected to migrate 440 m in 10 years in the absence of biodegradation reactions. Oxygen depletion extends well beyond the hydrocarbon plume, which can be explained by the secondary redox reactions that consume oxygen (*i.e.,* for the re-oxidation of CH_4, Fe^{2+} and Mn^{2+}). Likewise, both the primary and secondary redox reactions influence the pH and, thereby the fraction of dissolved inorganic carbon (DIC) that is present in the form of CO_2 (see Appendix A for gas concentrations).

Aerobic degradation and fermentation of benzene create acidic conditions and result in lower pH, while the reductive dissolution of manganese oxide and ferric iron minerals increase pH. At the same time, the reoxidation of CH_4, Fe^{2+} and Mn^{2+} lower the pH around the edge of their respective plumes. These opposing trends create a zone of maximum pH as reflected in the pCO_2 distribution (Appendix A), and Ca^{2+} concentration with dissolution and precipitation of calcite (not shown).

Other potential mechanisms that would result in the removal of dissolved Fe^{2+} and Mn^{2+} include the precipitation of siderite and rhodochrosite, respectively. The precipitation of these substances requires dissolved inorganic carbon. Given the separation between the zone of high DIC and the dissolved Mn^{2+} or Fe^{2+}, there is negligible precipitation of siderite and rhodochrosite. The formation of iron sulphide, not modeled, is another reaction that could remove dissolved Fe2+. The model simulations indicate the importance of oxygen on dissolved metals transport. Oxygen recharge along the flow path was simulated in the model but phase-transfer kinetics between the vadose and unsaturated zone are uncertain. The biogeochemical reactions that lead to the elongated Fe^{2+} and Mn^{2+} plumes are further discussed for Scenario 2 in the discussion section of the report.

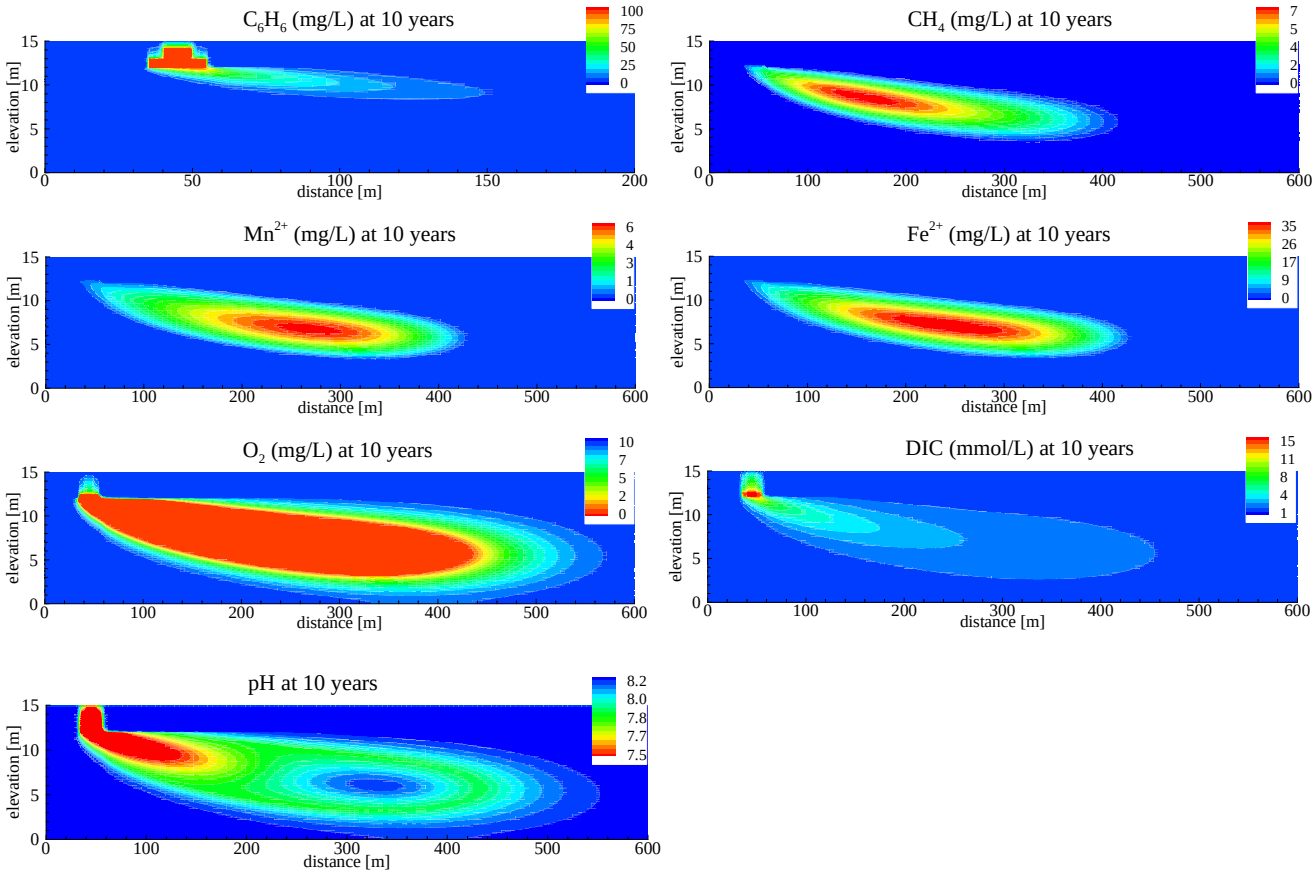

Figure 5: Baseline simulation results at 10 years showing the dissolved aqueous phase concentrations. Note that the distance is shown on different scales.

At 20 years simulation time, the results look similar in distribution and shape to 10 years, but the plume has advanced further, and the residual hydrocarbon remains in both the vadose zone and the capillary fringe. At 40 years simulation time; however, the residual hydrocarbon is depleted in the vadose zone, but persists in the capillary fringe past 50 years.

6.2.2 Effect of reduced groundwater and infiltration flow rates (Scenario 2)

In Scenario 2, the hydrogeological conditions were modified to result in reduced groundwater flow and infiltration rates that are consistent with the values simulated in the study of Mayer *et al.* (2002). The simulation results of Scenario 2 for the dissolved aqueous concentrations at 10 years simulation time are shown in Figure 6. The distribution of the different species evaluated is similar to Scenario 1.

With the reduced flow rates, the dissolved hydrocarbon plume is approximately 90 m long. The dissolved Fe^{2+} and Mn^{2+} plumes are approximately 160 m long (difference of 70 m). The Scenario 1 distances for dissolved hydrocarbon and Fe^{2+} and Mn^{2+} plumes were 120 m and 390 m, respectively (difference of 270 m). The ratio of the hydrocarbon to Fe^{2+}/Mn^{2+} plume lengths were 0.31 for Scenario 1 and 0.56 for Scenario 2. For Scenario 2, the distance between the centres (areas of maximum concentrations) of the hydrocarbon plume and the dissolved Fe^{2+} and Mn^{2+} plumes are also less compared to Scenario 1.

The results for Scenario 2 are compared to those of Mayer *et al.* (2002) in discussion section of the report (Section 7.0).

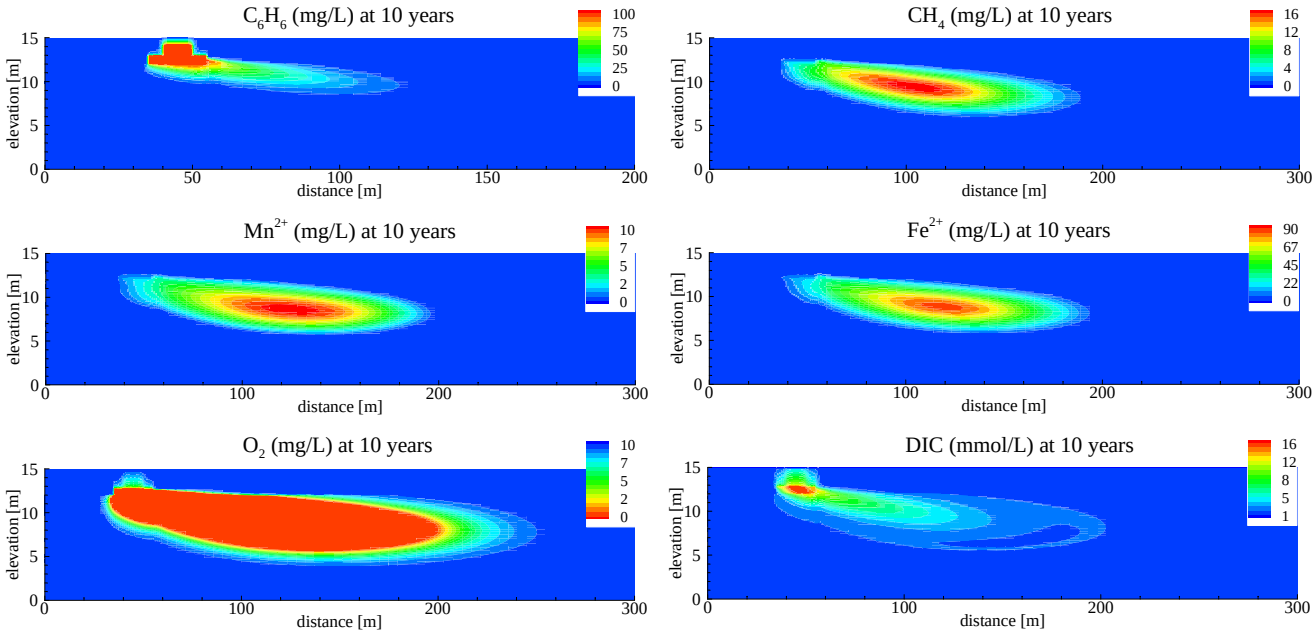

Figure 6: Scenario 2 simulation results at 10 years showing the dissolved aqueous phase concentrations. Note that the distance is shown on different scales.

6.2.3 Effect of thinner source on depletion (Scenario 3)

In Scenarios 1 and 2, the residual-phase hydrocarbon persists in the capillary fringe and the vadose zones of the source area after 10 years simulation time (and 40 years as discussed above). A third Scenario 3 was therefore considered in which the thickness of the LNAPL saturation in the capillary fringe is assumed to be 20 cm as compared to 1.0 m in Scenario 1.

The results indicate that despite the smaller initial volume of contamination between the two scenarios (2200 L for Scenario 1 versus 600 L in Scenario 3), the residual hydrocarbon persists to beyond 20 years in both the vadose zone and the capillary fringe for Scenario 3. Under the conditions simulated, the biodegradation, dissolution, and volatilization of the hydrocarbon, as well as the transport processes take longer than 50 years to deplete the hydrocarbon contamination.

The effect of the persistent hydrocarbon plume on the dissolved Fe^{2+} and Mn^{2+} is that their concentrations remain high, although they plateau at approximately 10 years simulation time (Figure 7). The predicted maximum Fe^{2+} and Mn^{2+} concentrations are lower than those predicted in the baseline Scenario 1 by 25% and 20%, respectively.

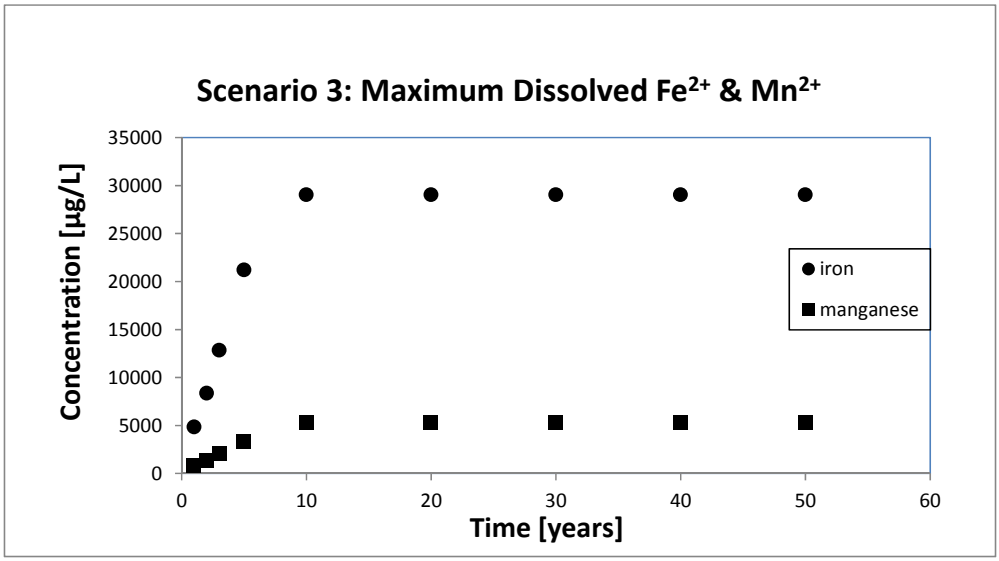

Figure 7: Transient evolution of maximum dissolved Fe^{2+} and Mn^{2+} in the model domain.

6.2.4 Effect of residual hydrocarbon source removal (Scenario 4)

In Scenario 4, the model is setup such that the residual hydrocarbon is removed at a constant rate with the result that it is completely depleted by 10 years simulation time in both the vadose zone and the capillary fringe. This scenario is analogous to mass reduction of hydrocarbon through enhanced bioremediation in the soil after 10 years of its presence in the subsurface. The resulting decline in the dissolved concentration of benzene is shown in Figure 8. The results indicate that the groundwater concentrations of benzene rapidly decrease and are completely depleted at the centre of the plume in approximately six months following the removal of the residual phase.

As shown in Figure 9, the dissolved Fe^{2+} and Mn^{2+} concentrations remain high for approximately five years following the removal of the residual hydrocarbon source. At 10 years following the removal of the source, the predicted maximum Fe^{2+} and Mn^{2+} concentrations decrease by approximately 35% and 50%, respectively.

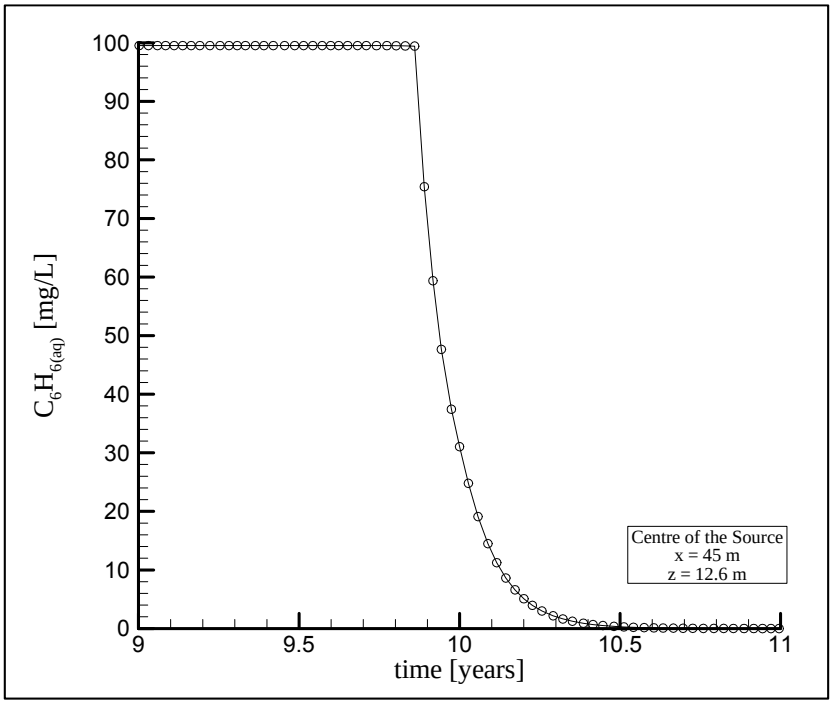

Figure 8: Transient evolution of dissolved benzene before and after the removal of the residual phase at 10 years simulation time.

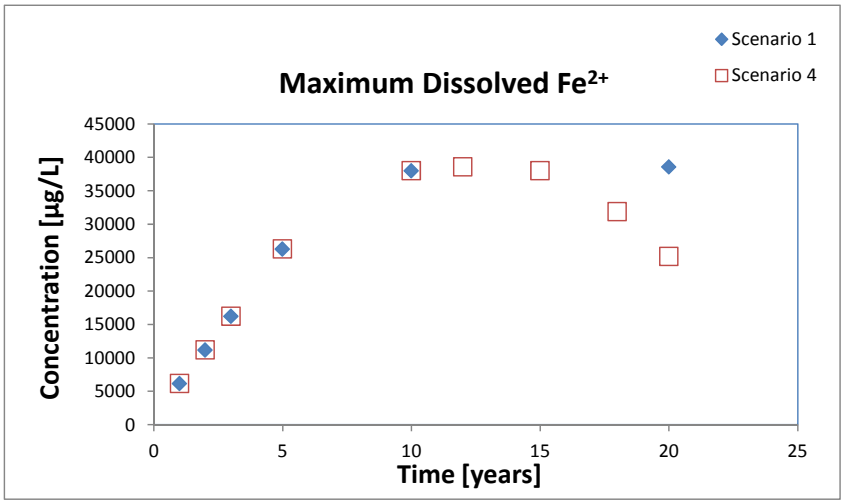

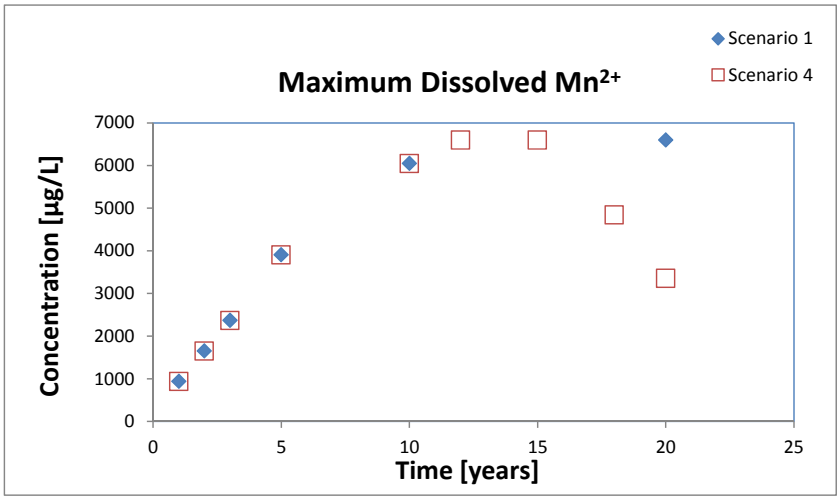

Figure 9: Maximum dissolved Fe^{2+} and Mn^{2+} concentrations for the baseline Scenario 1 and the source removal Scenario 4.

6.3 Effect of methane (Scenario 5)

In Scenario 5, methane generation from anaerobic degradation of benzene (R_{pr5}) is set to zero in order to evaluate the effect of methane on hydrocarbon and dissolved Fe^{2+} and Mn^{2+} plumes. The absence of methane generation would be realistic for certain sites with redox conditions not conducive of fermentation. The results for the aqueous phase concentrations are shown in Figure 10. In the absence of methane generation, the hydrocarbon plume length is 270 m as compared to 120 m in Scenario 1 (a difference of 150 m). While there is little difference in the dissolved Fe^{2+} and Mn^{2+} plume lengths between Scenario 1 and 5, the maximum concentration of dissolved Fe^{2+} in Scenario 5 is approximately 40% lower than in Scenario 1.

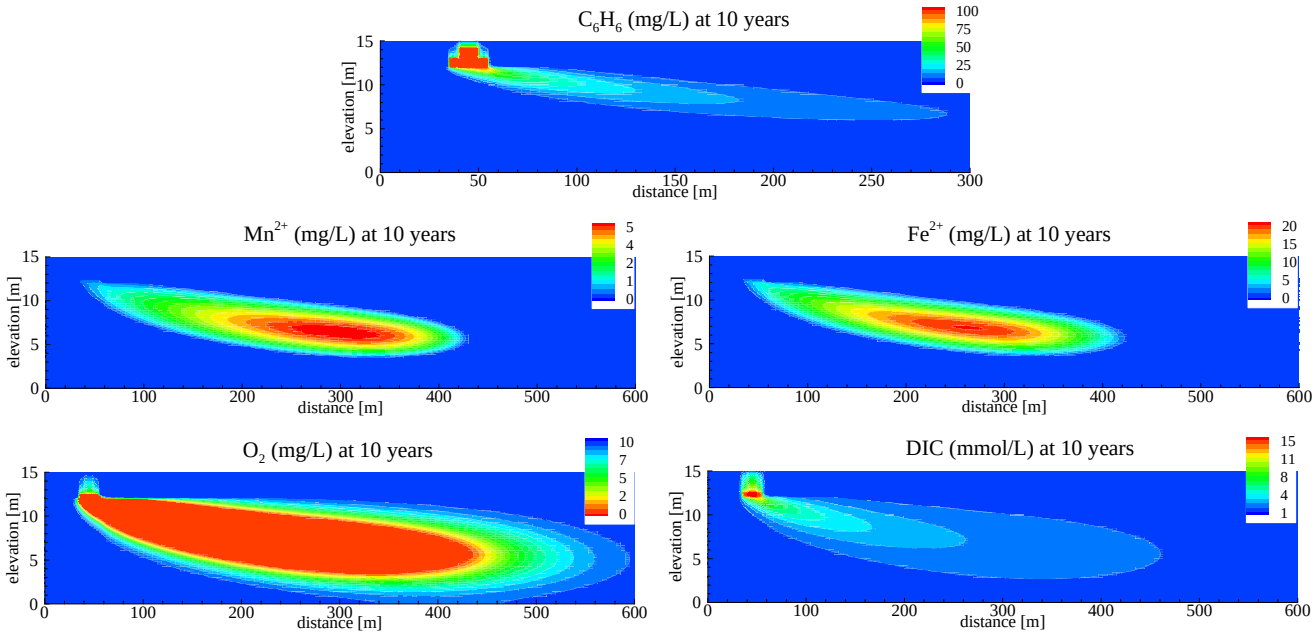

Figure 10: Scenario 5 simulation results at 10 years showing the dissolved aqueous phase concentrations. Note that the distance is shown on different scales.

6.4 Three-dimensional simulation (Scenario 6)

A three-dimensional simulation (Scenario 6) was conducted to assess the effects of dimensionality on plume lengths. Scenario 6 has the same model input parameters as Scenario 2 (reduced flow rates), with the added dimension in the transverse horizontal dimension (y). The simulation is set up in half-space with the centre of the plume at y = 0. The hydraulic conductivity and dispersivity in the transverse horizontal dimension (y) are assumed to be the same as for the transverse vertical dimension (z). The residual hydrocarbon source in the capillary fringe and the vadose zone are assumed to extend the same distance in x and y direction.

The dissolved concentrations of benzene and Fe^{2+} are shown in Figure 11 in three-dimensions. The extent of the benzene and iron plumes in the y direction is approximately 12 m from the plume centre (*i.e.,* the concentrations are 1% of their respective maxima at y = 12 m). In the x direction, the lengths of the plumes are similar to the Scenario 2 results in two dimensions (Figure 12). The benzene plume is 85 m long as compared to 90 m in Scenario 2, however, given the grid spacing of 5 m, this is a negligible difference. The dissolved Fe^{2+} and Mn^{2+} plumes are slightly greater than in Scenario 2 at approximately 185 m as compared to 160 m. This difference is also negligible given the coarser grid spacing of 10 m at the leading edge of the dissolved Fe^{2+} and Mn^{2+} plumes.

The concentrations of methane, dissolved Fe^{2+} and Mn^{2+} are lower than in Scenario 2 with their maximum concentrations being 11 mg/L, 57 mg/L, and 8.0 mg/L, respectively, in Scenario 6 (decrease of 35%, 34%, and 27%, respectively, from Scenario 2). Further discussion of the Scenario 6 results are provided in Section 7.0.

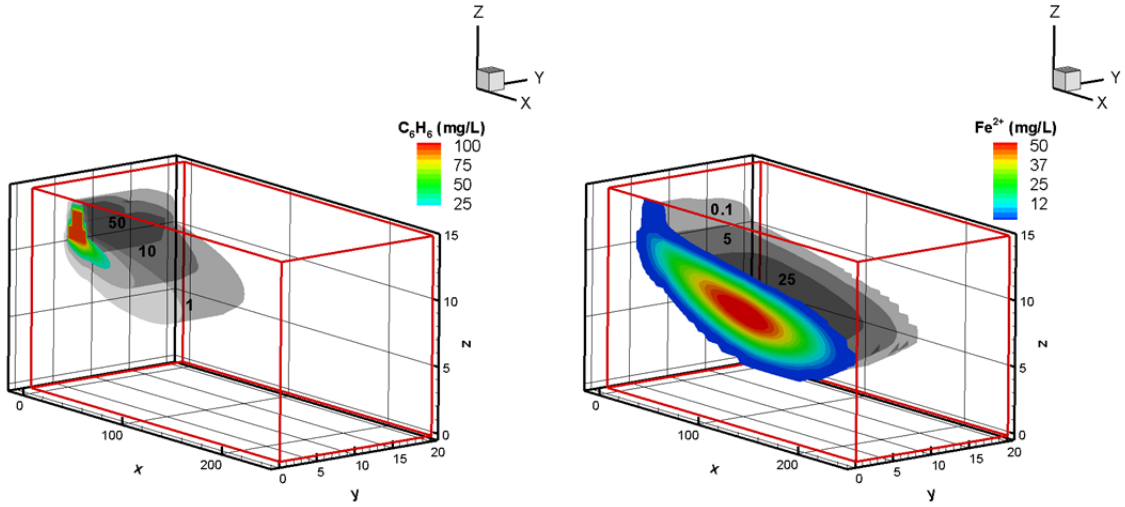

Figure 11: Benzene and dissolved Fe^{2+} plumes in three-dimension, z is the elevation, x is the horizontal distance in the direction of groundwater flow, and y is the transverse horizontal distance.

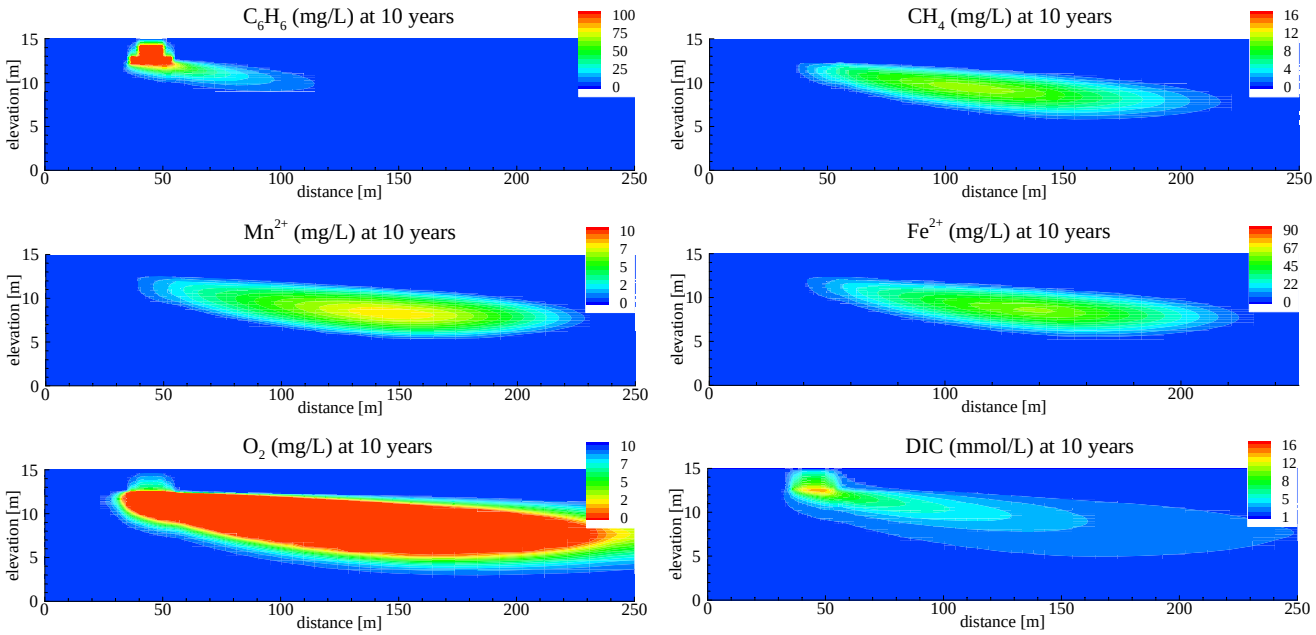

Figure 12: Vertical cross-section (y = 0) of simulation results at 10 years showing the dissolved aqueous phase concentrations for Scenario 6.

7.0 DISCUSSION OF MODEL RESULTS

The numerical model MIN3P-DUSTY was used in simulating the fate and transport of a residual hydrocarbon source in the vadose zone and the capillary fringe of a sandy aquifer following the conceptual site model previously defined. The input parameters to the model are mostly based on the simulations presented in the study of Mayer *et al.* (2002). However, consideration was given to the hydrogeological and geochemical conditions of the Lower Mainland region. Nitrate and sulphate in the background groundwater were not considered in this study, although there may be elevated concentrations in the Lower Mainland region near agricultural areas, and areas influenced by seawater, respectively. Therefore, some input parameter values related to soil properties and hydraulic gradient, as well as the soil content of iron and manganese minerals were altered to better reflect regional conditions.

7.1 Comparison to Mayer *et al.* (2002)

Because the simulation of a petroleum hydrocarbon release in Mayer *et al.* (2002) forms the basis for this modelling study, an effort was made to compare and interpret the simulation results of this study (Scenario 2) with those presented in Mayer *et al.* (2002). Both models consider the presence of residual LNAPL saturation in the vadose zone (1% saturation and 10 m long in direction of groundwater flow), and in the capillary fringe (10% saturation with thickness of 1 m and 20 m long).

The simulation results of Mayer *et al.* (2002) show a hydrocarbon (toluene) plume length of approximate 100 m and a longer dissolved Fe^{2+} plume of approximately 170 m. The methane plume is slightly shorter than the Fe^{2+} plume with the maximum methane concentration located near the centre of the plume, whereas the maximum dissolved Fe^{2+} concentrations are predicted at the hydrocarbon source zone. For Scenario 2, the same average groundwater velocity (16 m/year) and infiltration rate (200 mm/year) was assumed as for Mayer *et al.* (2002). The Scenario 2 results are plume lengths (90 m for benzene and 160 m for dissolved Fe^{2+}) that are consistent with those in Mayer *et al.* (2002). However, the Scenario 2 plume shape and location of maximum Fe^{2+} concentration (which is similar to Scenario 1) is different than the Mayer *et al.* (2002) simulations.

The likely primary reason for the difference in plume shape and distribution of reduced species is that the goethite and ferrihydrite volume fractions selected in this study (Table 5) are a factor of 250 times greater than those assumed in the study of Mayer *et al.* (2002), and are not a limiting factor in the reductive dissolution reactions and remain at high concentrations through the 50 years simulation time. In contrast, goethite and ferrihydrite are predicted by Mayer *et al.* (2002) to be depleted within the hydrocarbon plume after ten years, which is consistent with observations. The iron and manganese mineral contents for this study were based on recent literature and are considered representative values.

Other differences between simulations in this study and that in Mayer *et al.* (2002) are 1) shallower water table depth (by 3 m); 2) inclusion of hydrocarbon degradation through reductive dissolution of manganese oxides and subsequent re-oxidation of the dissolved Mn^{2+}; 3) higher dispersivity in the vertical and horizontal direction (by a factor of 10); and 4) inclusion of absorption of petroleum hydrocarbon into organic carbon was included for this study. Simulations with greater depth to water table, removal of manganese, and lower dispersivity showed little difference in the shape and length of the dissolved Fe^{2+} plume (results not shown).

Under conditions simulated in Mayer *et al.* (2002), high concentrations of dissolved Fe^{2+} are present in the anaerobic zone created near the source zone, where in combination with the produced DIC, the conditions are favourable for the precipitation of the Fe carbonate mineral (siderite). Although, mineral precipitation and dissolution reactions were considered in this study, siderite (and rhodochrosite) precipitation is not predicted in contrast to the results of Mayer *et al.* (2002). This can be explained by the separation in locations of predicted high concentration zones of DIC and dissolved Fe^{2+} and Mn^{2+} (Figures 5 and 6).

Overall, there is relatively good correspondence between this study and Mayer *et al.* (2002), when there is a closer match in input parameters, for example in Scenario 2, which increases the confidence in the modeling results of this study.

7.2 Plume longevity and effects of LNAPL source removal

Simulations were conducted to evaluate the natural attenuation of the hydrocarbon plume for the thinner residual LNAPL source zone in the capillary fringe (Scenario 3) or in the case of the removal of the residual LNAPL hydrocarbon (Scenario 4).

The results of the thinner source indicated that LNAPL persists in both the vadose zone and the capillary fringe beyond 20 years. Similar results were obtained between Scenario 1 and 3, in that LNAPL in the vadose zone was depleted by 40 years simulation time (between 30 and 40 years), whereas the LNAPL at the capillary fringe remained beyond 50 years simulation time. The key effect of the thinner LNAPL source in capillary fringe was in lower dissolved Fe^{2+} and Mn^{2+} concentrations predicted for Scenario 3 (Figure 7) by 25% and 20%, respectively.

The slow removal of the LNAPL source from the vadose and capillary fringe between zero and ten years was simulated for Scenario 4. The results indicate relatively fast attenuation of the dissolved benzene (Figure 8) in approximately six months. The dissolved Fe^{2+} and Mn^{2+} concentrations are predicted to persist at nearly constant and high concentrations for another five years. At 15 years simulation time (five years following hydrocarbon source removal), the concentrations of dissolved Fe^{2+} and Mn^{2+} begin to decline, and are lower by 35% and 50%, respectively, at 10 years following hydrocarbon source removal (Figure 9).

7.3 Methane generation and oxidation

The results of Scenario 5 show that in the absence of methanogenesis, the hydrocarbon plume is elongated by 150 m, while there is no change in the dissolved Fe^{2+} and Mn^{2+} plume lengths. A possible explanation is that methanogenesis is partly compensated by an increase in the reductive dissolution of iron hydroxide and manganese oxide minerals for benzene oxidation. However, there is no increase in the dissolved Fe^{2+} and Mn^{2+} concentrations, since there is no reductive dissolution of these minerals for the oxidation of methane as compared to Scenario 1. In fact, there is a decrease in the predicted concentrations of the dissolved Fe^{2+} and Mn^{2+}.

7.4 Three-dimensional simulation

In a two-dimensional simulation, the surface of the hydrocarbon plume exposed to oxic conditions is reduced relative to a more realistic three-dimensional representation of the plume. Previous modelling studies have shown that under certain conditions, there can be significant differences in the two- and three-dimensional predicted concentrations and plume lengths of hydrocarbons (*e.g.,* Molson *et al.*, 2002). To test the dimensionality effect on the simulation results in this study, a three-dimensional simulation (Scenario 6) was conducted based on the model setup for Scenario 2. Scenario 2 was selected for this comparison in order to limit the domain size (*i.e.,* shorter plume lengths) because larger domains require excessive model run times (*i.e.*, days).

The results indicate negligible differences in plume lengths between Scenarios 2 and 6, however, the concentrations of the reduced species, methane, dissolved Fe^{2+} and Mn^{2+} are lower by approximately 30%. Under the conditions simulated in this study, the impact of dimensionality on the results is relatively low. One reason could be the low dispersivity value selected for the transverse horizontal direction (*i.e.,* equal to that of the transverse vertical direction), although the dispersivity values chosen in this study are relatively high. Other possible factors are the size of the hydrocarbon source zone and consideration of anaerobic degradation pathways. For example, in the study of Molson *et al.* (2002), in which dimensionality has a significant effect on the predicted benzene plume, only aerobic degradation of benzene is considered, and the hydrocarbon source width (in the transverse horizontal direction) is assumed to be 1 m (10 m is the width assumed in this study). Furthermore, the simplifying assumption of a homogeneous aquifer is unlikely to reflect actual site conditions for either the two-dimensional or the three-dimensional Scenarios.

7.5 Comparison to CSR drinking water standards and of plume lengths

The maximum dissolved iron concentrations in the plume exceed the CSR DW standard of 6,500 µg/L by factors ranging from 3.1 to 13 (Table 8) and maximum dissolved manganese concentrations exceed the DW standard of 550 µg/L by factors ranging from 6.0 to 19. Scenario 5 with no methane generation results in the lowest ratio of maximum dissolved iron predicted to the DW standard, while a decrease in groundwater flow and infiltration rates result in the highest ratios of 13 and 8.8 for Scenarios 2 and 6, respectively.

The dissolved Fe^{2+} plume is longer than the benzene plume by a factor of 1.4 to 3.8 in all scenarios simulated (Table 8). The dissolved Mn^{2+} plume lengths were similar to the dissolved iron.

Table 8: Maximum dissolved iron and manganese concentrations compared to CSR Schedule 6 standard for Drinking Water and relative plume lengths for dissolved iron at 10 years simulation time.

Scenario	Max. [Fe^{2+}] (µg/L)	Ratio of Max. [Fe^{2+}] to CSR DW standard	Fe^{2+} plume length (relative to benzene)	Max. [Mn^{2+}] (µg/L)	Ratio of Max. [Mn^{2+}] to CSR DW standard
1. Baseline	38,000	5.8	3.3	6,200	11
2. Reduced flow rates	87,000	13	1.8	11,000	19
3. Thinner source	29,000	4.4	3.8	5,300	9.6
4. Source removal[1]	25,000	3.8	-	3,300	6.0
5. Effect of methane	20,000	3.1	1.4	5,300	9.6
6. Three dimensional (this simulation relative to Scenario 2)	57,000	8.8	2.2	8,000	15

[1] Results are shown for 10 years following the removal of residual free phase hydrocarbon (20 years simulation time).

7.6 Uncertainty in modelled Fe^{2+} and Mn^{2+} predictions

The possible precipitation of iron sulfide minerals is not included in the model. The importance of this reaction will depend on available sulfate in an aquifer, which may be elevated where there is a salt-water wedge, in agricultural areas or where soils are high in gypsum content. Modeling of iron sulphide precipitation or redox reactions is challenging because of limited reaction rate data.

Oxygen recharge through vadose zone diffusion and oxygenated infiltrating water is included in the model. However, more complex processes (which cannot be currently simulated) such as water table fluctuations leading to the entrapment of oxygen could increase oxygen transfer to the saturated zone, and methane flux to the unsaturated zone through ebullition could reduce methane concentrations in groundwater. This latter process was found to be significant at the Bemidji site (Amos and Mayer, 2006), although methane concentrations predicted for this study were lower and likely not sufficient to lead to significant ebullition. Another factor that would lead to increased oxygen transfer is mixing and diffusion across stratigraphic layers with varying hydraulic conductivities (*i.e.*, dual porosity effect due to aquifer heterogeneity). These processes would tend to reduce dissolved iron and manganese concentrations in groundwater.

The dissolved Fe^{2+} and Mn^{2+} plume is assumed not to absorb to aquifer materials. In contrast, the benzene plume advancement is not only subject to aerobic biodegradation, but also absorption into organic carbon. Based on the DIC zonation, the formation of siderite and rhodochrosite does not occur, but there may be other types of sorption or precipitation of Fe^{2+} and Mn^{2+}.

The model-predicted Fe^{2+} and Mn^{2+} plume extents were not significantly different. With the additional processes described above, it is possible that the predictions would have shown greater plume extents for manganese compared to iron, which would be consistent with measurement data by Christensen *et al.* (2000) for the Grindsted landfill where the reduced iron plume migrated 230 m from the source, and where the reduced manganese plume migrated over 300 m.

Modelling of above processes is either not feasible or was not possible within the project scope. A sensitivity analysis involving simulations where ranges of key inputs considered in modelling (*e.g.*, mineral iron and manganese content, reaction rates) and above factors (iron sulphide precipitation, sorption) would provide useful information.

8.0 OVERVIEW OF MANAGEMENT OPTIONS FOR IRON AND MANGANESE

Potential management options for sites with iron and manganese above levels of concern include risk assessment, *in situ* treatment, and ex situ treatment of extracted groundwater (when drinking water quality is of concern).

Technologies involving oxic *in situ* treatment of petroleum hydrocarbons will by nature increase the oxygen in the aquifer and decrease the potential for migration of reduced species such as iron and manganese. Such technologies can include air sparging, ozonation, oxidants such as sodium persulfate, and oxygen-release amendments such as calcium oxihydroxides.

A literature search revealed only limited published case studies involving *in situ* treatment technologies specific to iron and manganese. Once such technology “Vyredox” developed in Finland, involves the injection of air to stimulate iron-oxidizing bacteria and oxidation of Fe^{2+} to Fe^{3+} (Hallberg and Martinell, 1976). The method was developed to protect drinking water wells by installing a ring of injection wells around a drinking water well. Water that is oxygenated is injected into the formation to precipitate iron and manganese. This technology must be carefully implemented to avoid reduced soil permeability and clogging of wells and the aquifer surrounding the injection wells. Formation of slimes may also occur in pumping wells. For coarse-grained soils, clogging is less likely than for fine-grained soils. A potential technique to reduce the potential for clogging is to include a metals chelator in water such as polyphosphate to keep metals in solution. The literature search indicated that more recent documentation of the Vyredox technology uncovered was limited to short internet references to the use of this technology to treat iron and manganese in groundwater at aquifers in Long Island, New York; Cape Girardeau, Missouri; and Rib Mountain, Wisconsin.

There are common, commercially available and economically-feasible treatment options to remove iron and manganese from drinking water (CSAP, 2011). Treatment technologies for reduction of iron and manganese in water include aeration followed by filtration, adsorption systems, greensand filtration, ion exchange, and reverse osmosis. The effectiveness of each method often depends on the type of iron or manganese present, the

concentration, and the pH of the water. The driver for treatment of groundwater for iron and manganese is the aesthetic-based iron and manganese drinking water guidelines provided by Health Canada, which are approximately one order of magnitude less than the current toxicologically-based CSR DW standards. The benefit of lower aesthetic-based guidelines is that there would tend to be visual indicators such as staining of plumbing fixtures and "rusty" taste and look to the water before toxicological standards are reached.

9.0 CONCLUSIONS AND RECOMMENDATIONS

The numerical model MIN3P-Dusty was used to simulate the development of a hydrocarbon contaminant plume in groundwater and the unsaturated zone. The dissolution, volatilization, and biodegradation of the hydrocarbon (represented by benzene) under steady state flow conditions were considered as the controlling factors for the natural attenuation of the benzene plume. Aerobic biodegradation of benzene and anaerobic degradation pathways (manganese-reduction, iron-reduction, and methanogenesis) were considered along with re-oxidation of dissolved Fe^{2+} and Mn^{2+}, and methane.

A baseline scenario is defined with five additional scenarios to assess the effects of groundwater flow and infiltration rates; thinner source zone; removal of the residual LNAPL hydrocarbon; methane generation; and dimensionality (three-dimensional simulation). The lowest dissolved Fe^{2+} and Mn^{2+} concentrations are predicted when the degradation of benzene through methanogenesis is not considered, and highest concentrations developed in the scenarios with lower groundwater flow and infiltration rates.

The following conclusions on modeling results are drawn with respect to the project objectives:

- *Better understand natural attenuation processes of Fe^{2+} and Mn^{2+}*: The results are valuable in that they highlight the importance of the combination of contamination source characteristics, geochemical factors and hydrogeologic conditions on Fe^{2+} and Mn^{2+} fate and transport. The importance of primary and secondary oxidation-reduction reactions on redox conditions and Fe^{2+} and Mn^{2+} persistence is demonstrated. Oxygen and redox are important indicators of potential for Fe^{2+} and Mn^{2+} persistence.
- *Relative extent of Fe^{2+} and Mn^{2+} and petroleum hydrocarbon plumes*: Comparison of the plume lengths at 10 years simulation time showed that the dissolved Fe^{2+} and Mn^{2+} plumes extend further from the source than the benzene plume with plume length ratios ranging from 1.4 to 3.8 for the scenarios considered.
- *Longevity of Fe^{2+} and Mn^{2+} plumes once petroleum hydrocarbon source zones are remediated*: Once the residual hydrocarbon is removed, the attenuation time of the dissolved benzene plume is approximately six months. The dissolved Fe^{2+} and Mn^{2+} concentrations, however, remain relatively constant for five years following hydrocarbon source removal, and decrease by 35% and 50%, respectively, at ten years.
- *Comparison of Fe^{2+} and Mn^{2+} concentrations to CSR DW standards*: The maximum predicted concentrations of dissolved Fe^{2+} and Mn^{2+} exceed the DW standards by approximately half to one order of magnitude for scenarios representative of more typical aquifer conditions.

The modeling results suggest that Fe^{2+} and Mn^{2+} plumes may be more extensive than petroleum hydrocarbon plumes and that elevated concentrations may persist for an extended period of time after hydrocarbon sources are removed. The modeling results with respect to Fe^{2+} and Mn^{2+} plume lengths are likely somewhat conservative because certain processes (that are challenging to model because of limited data) such as sorption of reduced iron or precipitation of iron sulphides were not included.

A literature search indicated limited case studies with data enabling comparison of the transport of petroleum hydrocarbons and iron and manganese in groundwater. One study of municipal landfill leachate indicated dissolved Fe^{2+} and Mn^{2+} concentrations that were highly elevated, had migrated long distances, and extended well beyond the BTEX plume. In contrast, the plume scale data for the Bemidji, Minnesota site show the plume lengths of iron and BTEX compounds were well correlated (*i.e.*, similar).

An inference from the modeling results and landfill case study is that landfill leachates and larger petroleum hydrocarbon sources will have greater potential to create reducing zones and elevated iron and manganese concentrations and longer dissolved iron and manganese plumes. For smaller sources representative of many petroleum hydrocarbon releases at gasoline station sites there is expected to be less potential for significant impacts to drinking water from iron and manganese based on the modeling results for scenarios where a smaller hydrocarbon source or source removal were simulated, which predicted lower iron and manganese concentrations.

Other processes not considered in this study that could potentially reduce the plume lengths are water table fluctuations and reduced permeability in zones of high gas generation (*i.e.*, methanogenic zones). Amos and Mayer (2006) show that water fluctuations could result in the entrapment of bubbles containing atmospheric (oxygenated) gases that could result in further oxidation reactions. In addition, Amos and Mayer (2006) also consider the reduction in permeability caused by an increase in dissolved gas concentrations in the methanogenic zone that can limit plume expansion.

The modeling results are also instructive in providing insight on time scales for natural attenuation of LNAPL sources and indicate that many decades may be needed for source zone depletion. This may have potential implications for policy on allowable timescales for natural attenuation (*e.g.*, BC MoE Technical Guidance 22).

The modeling is specific to the scenarios considered and certain simplifying assumptions were made considering the highly complex nature of the processes simulated. Knowledge of site conditions and inputs consistent with such conditions would be necessary for a better understanding of plume development at a specific site. With hopefully added future experience with respect to model calibration, there is the potential to use MIN3P or similar model on site and project specific basis to better understand iron and manganese fate and transport.

Recommendations for further research include model comparisons to field data at well characterized sites, and modeling studies where key processes and inputs are varied and additional processes are considered. This could include simulation of sequential oxidation-reduction processes, inclusion of sorption of Fe^{2+} and Mn^{2+}, inclusion of denitrification, sulphate reduction and FeS_2 precipitation, and Fe^{2+} oxidation by reductive dissolution of MnO_2. However, parameterization of these processes is highly uncertain and therefore modeling is not straightforward. Consideration could be given to varying the goethite and ferrihydrite volume fractions, but further research would be required to determine appropriate input parameter values.

10.0 CLOSURE

We trust the above report meets your requirements at this time should you have any questions please contact the undersigned.

GOLDER ASSOCIATES LTD.

Parisa Jourabchi, Ph.D.
Environmental Scientist

Ian Hers, Ph.D., P.Eng.
Principal

o:\final\2012\1436\12-1436-0089\1214360089-001-r-rev0 csap draft fe and mn_05dec_2013.docx

11.0 REFERENCES

Amos, R. T., and K. U. Mayer (2006). “Investigating the role of gas bubble formation and entrapment in contaminated aquifers: Reactive transport modelling.” Journal of Contaminant Hydrology **87**:123-154.

Amos, R. T., B. A. Bekins, et al. (2011). “Methane oxidation in a crude oil contaminated aquifer: Delineation of aerobic reactions at the plume fringes.” Journal of Contaminant Hydrology **125**: 13-25.

Amos, R. T., B. A. Bekins, et al. (2012). “Evidence for iron-mediated anaerobic methane oxidation in a crude oil-contaminated aquifer.” Geobiology **10**: 506-517.

ASTM (2004). Standard Guide for Remediation of Ground Water by Natural Attenuation at Petroleum Release Sites. Designation E 1943-98 (Reapproved 2004).

Baedecker, M. J., I. M. Cozzarelli, et al. (1993). "Crude oil in a shallow sand and gravel aquifer - III. Biogeochemical reactions and mass balance modeling in anoxic groundwater." Applied Geochemistry **8**: 569-586.

Bolton, M. (2004). Aqueous and Mineralogical Analysis of Arsenic in the Reduced Circumneutral Groundwaters and Sediments of the Fraser River Delta, British Columbia. Department of Earth and Ocean Sciences. Vancouver, University of British Columbia. **Master of Science:** 167pp.

Chapelle, F. H. (1993). Ground-Water Microbiology and Geochemistry. New York, Wiley.

Christensen, T. H., P. L. Bjerg, et al. (2000). "Characterization of redox conditions in groundwater contaminant plumes." Journal of Contaminant Hydrology **45**(3-4): 165-241.

CSAP (2011). TG6 Working Group Report: Iron and Manganese Drinking Water Use Standards, CSAP Technical Review # 1101, December 16, 2011.

Essaid, H. I., B. A. Bekins, et al. (2011). "Crude oil at the Bemidji site: 25 years of monitoring, modeling, and understanding." Ground Water **49**: 706-726.

Golder Associates Ltd. (2005). Preliminary Evaluation of the Suitability of Fraser River Sands as Fill Material in the Vicinity of Burns Bog. Burnaby**:** 18.

Jackson, R. E., V. Dwarakanath, et al. (2006). "Migration of viscous non-aqueous phase liquids (NAPLs) in alluvium, Fraser River lowlands, British Columbia." Canadian Geotechnical Journal **43**: 694-703.

Essaid, H. I., I. M. Cozzarelli, et al. (2003). "Inverse modeling of BTEX dissolution and biodegradation at the Bemidji, MN crude-oil spill site." Journal of Contaminant Hydrology **67**(1-4): 269-299.

Hallberg, R.O. and R. Martinell, 1976. Vyredox – In Situ Purification of Ground Water. Ground Water. **14(2)**.

Hunter, K. S., Y. Wang, et al. (1998). "Kinetic modeling of microbially-driven redox chemistry of subsurface environments: coupling transport, microbial metabolism and geochemistry." Journal of Hydrology **209**: 53-80.

Katsev, S., D. G. Rancourt, et al. (2004). "dSED: a database tool for modeling sediment early diagenesis." Computers & Geosciences **30**: 959-967.

Kissel, J.C., 1985. “Numerical simulation of mixed-culture biofilms.“ Ph.D. thesis, Stanford University, Stanford, California.

Madigan, M.T., J.M. Martinko, D.P. Clark, and D.A. Stahl. 2010. “Brock’s Biology of Microorganisms.” Prentice Hall, NJ.

Masue-Slowey, Y., B. D. Kocar, et al. (2011). "Transport implications resulting from internal redistribution of arsenic and iron within constructed soil aggregates." Environmental Science & Technology **45**: 582-588.

Mayer, K. U., E. O. Frind, et al. (2002). "Multicomponent reactive transport modeling in variably saturated porous media using a generalized formulation for kinetically controlled reactions." Water Resources Research **38**: doi:10.1029/2001WR000862.

Molins, S. and K. U. Mayer (2007). "Coupling between geochemical reactions and multicomponent gas and solute transport in unsaturated media: A reactive transport modeling study." Water Resources Research **43**: doi:10.1029/2006WR005206.

Molins, S., K. U. Mayer, et al. (2010). "Vadose zone attenuation of organic compounds at a crude oil spill site - Interactions between biogeochemical reactions and multicomponent gas transport." Journal of Contaminant Hydrology **112**: 15-29.

Molson, J. W., J. F. Barker, and E. O. Frind (2002). "Modeling the impact of ethanol on the persistence of benzene in gasoline-contaminated groundwater." Water Resources Research **38**: doi: 10.1029/2001WR000589.

Morasch, B., D. Hunkeler, et al. (2011). "Intrinsic biodegradation potential of aromatic hydrocarbons in an alluvial aquifer - Potentials and limits of signature metabolite analysis and two stable isotope-based techniques." Water Research **45**(15): 4459-4469.

Neilson-Welch, L. and L. Smith (2001). "Saline water intrusion adjacent to the Fraser River, Richmond, British Columbia." Canadian Geotechnical Journal **38**: 67-82.

Postma, D. (1993). "The reactivity of iron oxides in sediments: a kinetic approach." Geochimica Et Cosmochimica Acta **57**: 5027-5034.

Roychoudhury, A.N. and G.L. Merrett (2006). “Redox pathways in a petroleum contaminated shallow sandy aquifer: Iron and sulfate reductions.” Science of the Total Environment **366**: 262–274.

Rubin, J. (1983). "Transport of reacting solutes in porous media: Relation between mathematical nature of problem formulation and chemical nature of reactions." Water Resources Research **19**: 1231-1252.

Schulze-Makuch, D. (2005). "Longitudinal dispersivity data and implications for scaling behavior." Ground Water **43**: 443-456.

Science Advisory Board Contaminated Sites (SABCS) (2010) British Columbia Ministry of the Environment (BC MoE) Soil Vapour Intrusion. Developed by Golder Associates Ltd. Beta Version. April 10, 2010.

Suarez, M. P. and H. Rifai (2004). "Modeling natural attenuation of total BTEX and benzene plumes with different kinetics." Groundwater Monitoring & Remediation **24**: 53-68.

Testa and Jacobs, 2004. Oil Spills and Leaks. Handbook of Complex Environmental Remediation Problems (Chapter 9), McGraw-Hill.

Tillman, F. D. and J. W. Weaver (2007) “Temporal moisture content variability beneath and external to a building and the potential effects on vapor intrusion risk assessment.” Science of the Total Environment, **379**: 1-15.

Tufano, K. J., S. G. Benner, et al. (2009). "Aggregate-scale heterogeneity in iron (hydr)oxide reductive transformations." Vadose Zone Journal **8**: 1004-1012.

Valentine, K. W. G., P. N. Sprout, T. E. Baker and L. M. Lawkulich (Eds.) (1978). The Soil Landscapes of British Columbia, BC Ministry of Environment, Resource Analysis Branch. 197p. http://www.env.gov.bc.ca/soils/landscape/1.2climate.html

Philippe Van Cappellen and Y. Wang (1996). "Cycling of iron and manganese in surface transport and reaction of carbon, oxygen, nitrogen, sulfur, iron, and manganese." American Journal of Science **296**: 197-243.

US EPA (2004). User's guide for evaluating subsurface vapor intrusion into buildings. Office of Emergency and Remedial Response, EPA Contract Number: 69-W-02-33.

US EPA (2013) Petroleum Vapor Intrusion Database. http://www.epa.gov/oust/cat/pvi/PVI_DB_final.accdb. Accessed January 14, 2013.

Wiedemeier, T.H., H. S. Rifai, C.J. Newell and J.T. Wilson. 1999. Natural Attenuation of Fuels and Chlorinated Solvents in the Subsurface. John Wiley and Sons. 617 pg.

Zawadzki, W., D. W. Chorley, et al. (2002). "Capture-zone design in an aquifer influenced by cyclic fluctuations in hydraulic gradients." Hydrogeology Journal **10**: 601-609.

APPENDIX A

SCENARIO 1 GAS PHASE CONCENTRATIONS AND REACTION RATES

Partial Pressures of Gaseous Species

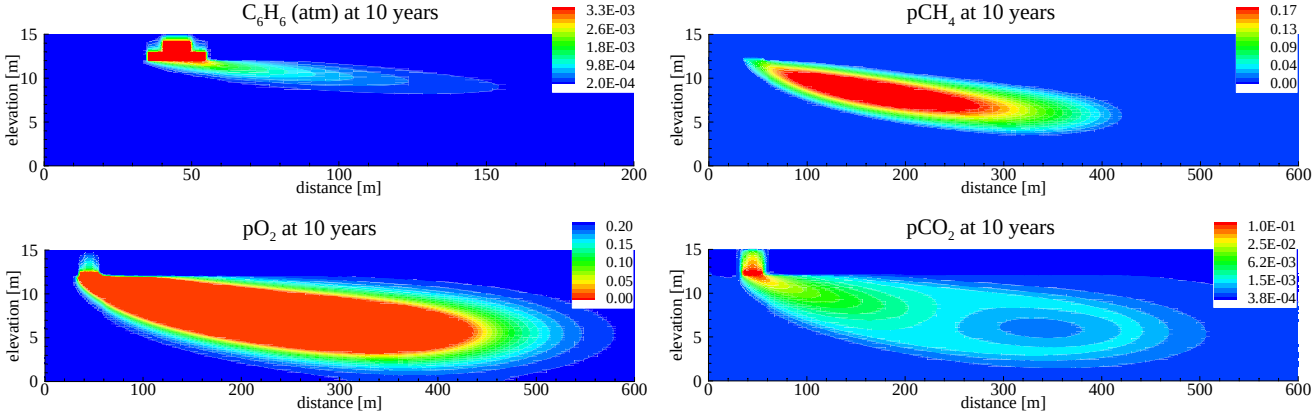

Reductive Dissolution Reaction Rates

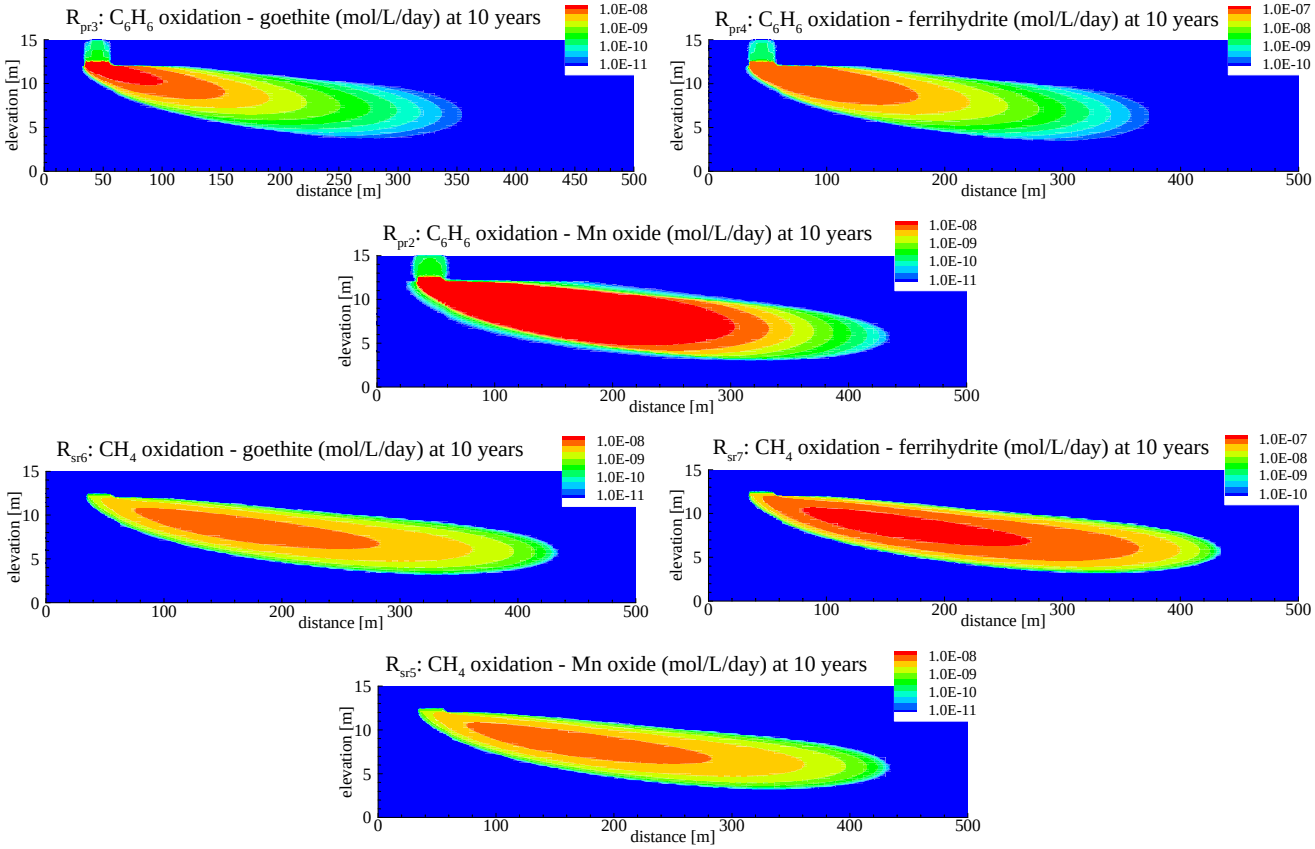

Intra-aqueous Redox Reaction Rates

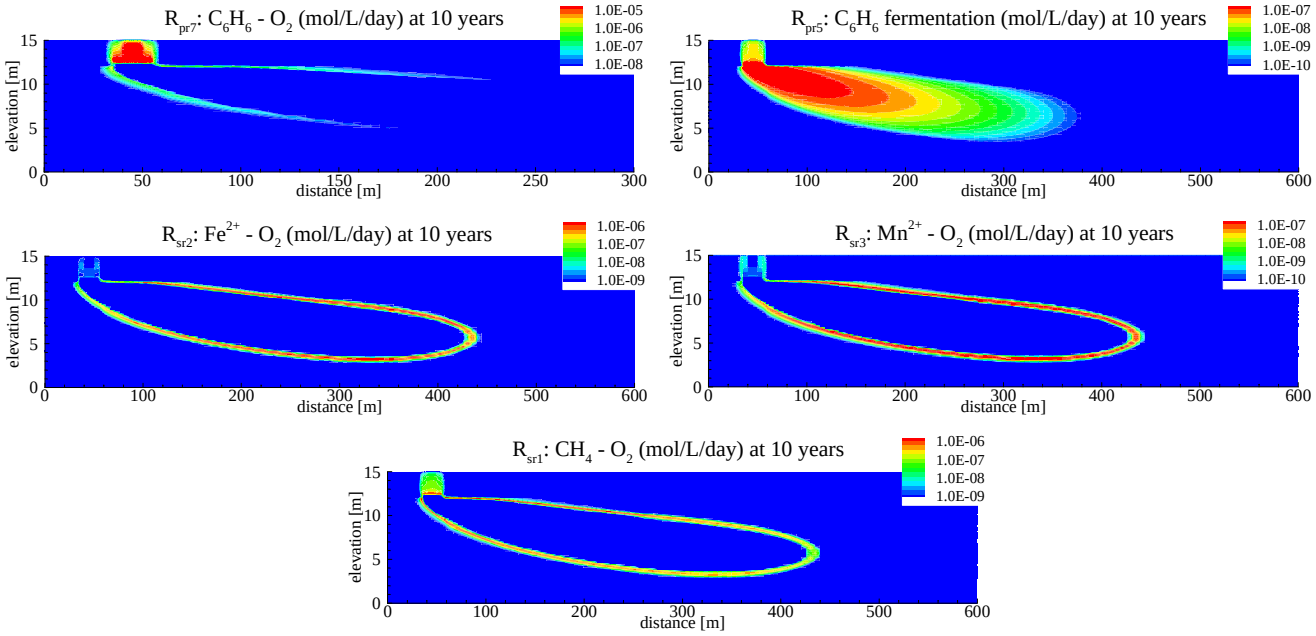

At Golder Associates we strive to be the most respected global company providing consulting, design, and construction services in earth, environment, and related areas of energy. Employee owned since our formation in 1960, our focus, unique culture and operating environment offer opportunities and the freedom to excel, which attracts the leading specialists in our fields. Golder professionals take the time to build an understanding of client needs and of the specific environments in which they operate. We continue to expand our technical capabilities and have experienced steady growth with employees who operate from offices located throughout Africa, Asia, Australasia, Europe, North America, and South America.

Africa	+ 27 11 254 4800
Asia	+ 86 21 6258 5522
Australasia	+ 61 3 8862 3500
Europe	+ 356 21 42 30 20
North America	+ 1 800 275 3281
South America	+ 55 21 3095 9500

solutions@golder.com
www.golder.com

Golder Associates Ltd.
500 - 4260 Still Creek Drive
Burnaby, British Columbia, V5C 6C6
Canada
T: +1 (604) 296 4200

Golder Associates